Immobilisation of Benzo[*c*][1,2,5]thiadiazole (BTZ) within Polymers of Intrinsic Microporosity (PIMs) for Use in Flow Photochemistry

Electronic Supplementary Information

Dominic Taylor,[a,b,†] John M. Tobin,[b,†] Leonardo Amicosante,[a] Andrew W. Prentice,[a] Martin J. Paterson,[a] Scott J. Dalgarno,[a,*] Neil B. McKeown,[b,*] and Filipe Vilela[a,*]

[a]School of Engineering and Physical Sciences, Heriot-Watt University, Riccarton, Edinburgh, EH14 4AS, UK.

[b]EaStCHEM School of Chemistry, University of Edinburgh, David Brewster Road, Edinburgh, EH9 3FJ, United Kingdom.

†These authors contributed equally.

*Corresponding authors.

E-mail: f.vilela@hw.ac.uk, neil.mckeown@ed.ac.uk, s.j.dalgarno@hw.ac.uk.

Table of Contents

1. General Experimental Details

All reagents and starting materials employed in this work were commercially available and used without further purification unless stated otherwise.

^{1}H NMR spectra of synthesised products were recorded using either a Bruker AVIII 300 spectrometer at 300 MHz or a Bruker AVIIIHD 400 MHz spectrometer in $CDCl_3$. Analysis of phosphine oxidation reactions was recorded using a Bruker AVIIIHD 400 MHz spectrometer using an inverse gated sequence, a D_1 of 40 s and an acquisition time of 2.5 seconds. ^{1}H and ^{13}C NMR spectra of polymers were analysed using a 500 MHz Bruker AVIIIHD spectrometer at ambient temperature in $CDCl_3$.

Solution-state UV-Vis spectra were recorded on a PerkinElmer Lambda 25 system with 10 mm quartz cuvettes using $CHCl_3$ as a solvent. Emission spectra were recorded using a Perkin-Elmer LS 55 fluorescence spectrometer in $CHCl_3$ as a solvent and 1 cm pathlength quartz cuvette. The excitation wavelength was the same as the wavelength of maximum absorption for each photosensitiser. Solid state UV-Vis absorption spectroscopy on the films was conducted using a ASCO V670 UV-VIS Spectrophotometer equipped with a reflectance spectroscopy integration sphere. Absorbance measured from 250-800 nm. Fluorescence microscopy on glass beads were carried out using a Zeiss Axiovert 200M with a 10x lens. Fabricated PIM films were examined using an optical microscope from LEEDs at 4x, 10x or 25x magnification.

Gas sorption measurements were carried out using a Quantachrome Quandrasorb Evo using N_2 at 77 K and CO_2 at 273 K. Samples were first outgassed at 100 ^{o}C for 24 h under vacuum using a Quantachrome FLOVAC degasser. TGA was measured using a TA SDT-Q600 analyser in the range of 25 – 800 ^{o}C under an atmosphere of nitrogen. IR spectra were recorded using a Shimadzu IRAffinity-1S Fourier Transform Infrared Spectrophotometer using powdered samples. Gel permeation chromatograms were recorded using a Agilent 1260 GPC from Agilent Technologies in THF solution using a refractive index detector.

Photosensitisation studies in batch were carried out by using a LED module emitting at 420 nm with 28 W light output and a light intensity of 3.5 W cm^{-2} (OSA Opto Lights, OLM-018 series, Berlin, Germany) at a distance of 7 cm.

2. Synthetic Details

Tetrakis(triphenylphosphine) palladium (0) and 4,7-dibromobenzo[*c*][1,2,5]thiadiazole were synthesised by literature procedures.[1,2] **pH-BTZ** and **ThTh-BTZ** were synthesised using a procedure reported by Taylor *et al*.[3] The monomer **EA** and **PIM-EA-TB** were synthesised according to literature methods reported by Carta *et al*.[4]

Di-*tert*-butyl-(benzo[*c*][1,2,5]thiadiazole-4,7-diylbis(4,1-phenylene))dicarbamate (pNHBoc-BTZ)

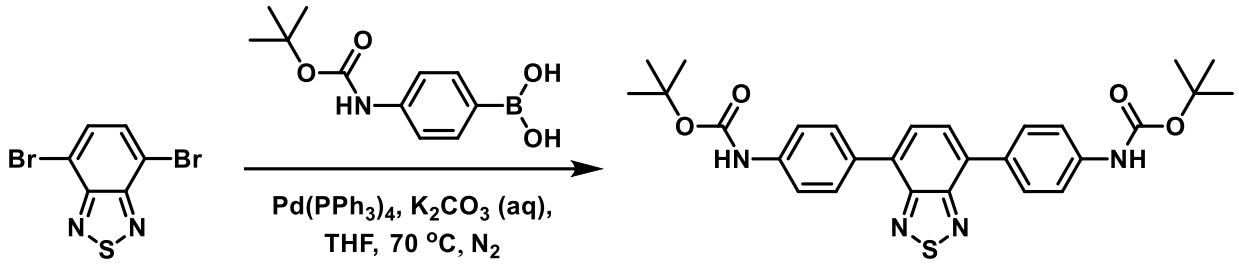

4,7-Dibromobenzo[*c*][1,2,5]thiadiazole (588 mg 2.0 mmol), *tert*-butyl-(4-(4,4,5,5-tetramethyl-1,3,2-dioxaborolan-2-yl)phenyl)carbamate (1.596 g, 5.0 mmol), potassium carbonate (830 mg, 4.0 mmol) and palladium tetrakis(triphenylphosphine) (0) (46 mg, 2 mol%) were added to a dry two-neck round bottom flask. The flask was evacuated and backfilled with nitrogen gas three times then degassed THF (40 mL) and degassed deionised water (5 mL) added. The reaction was heated to 70 ^{o}C under nitrogen for 16 hours then cooled to room temperature and poured onto deionised water (50 mL). The product was then extracted with DCM (3 x 25 mL) and the combined organic phases washed with deionised water (50 mL), dried over $MgSO_4$ then the solvent removed under reduced pressure. The crude product was then recrystallised from hot methylated spirits to yield yellow crystals (480 mg, 46%). **^{1}H NMR** ($CDCl_3$, 300 MHz, 25.0 ^{o}C) δ_H 7.93 (m, 4 *H*), 7.74 (s, 2 *H*), 7.54 (m, 4 *H*), 6.59 (bs, 2 *H*), 1.55 (s, 18 *H*). **^{13}C NMR** ($CDCl_3$, 75.5 MHz, 25.0 ^{o}C) δ_C 154.1, 152.6, 138.5, 132.4, 132.1, 129.9, 127.6, 118.5, 80.8, 28.4. **UV-Vis** ($CHCl_3$) λ_{max} (nm) 408. **IR** $\bar{\nu}$ (cm^{-1}) 3370 (m, N-H str.), 2980 (w, C-H str.), 1710 (m, C=O str.).

4,4'-(Benzo[*c*][1,2,5]thiadiazole-4,7-diyl)dianiline (pNH$_2$-BTZ)

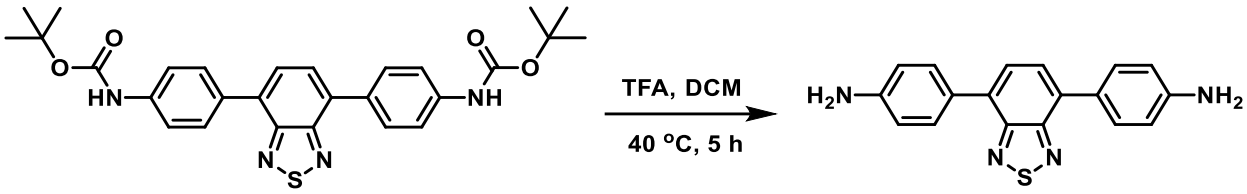

pNHBoc-BTZ (208 mg, 0.4 mmol) was dissolved in a mixture of DCM (20 mL) and trifluoroacetic acid (TFA) (0.4 mL, 32 mmol) then the solution was heated to 40 °C for 5 hours. Following this, the reaction mixture was poured onto water (100 mL) and the product extracted with ethyl acetate (3 x 50 mL). The combined organic layers were dried over $MgSO_4$ and the solvent was then removed under reduced pressure to yield the product as a red powder (110 mg, 87%). **^{1}H NMR** ($CDCl_3$, 300 MHz, 25.0 °C) δ_H 7.82 (m, 4 *H*), 7.77 (s, 2 *H*), 6.85 (m, 4 *H*), 3.84 (bs, 4 *H*). **^{13}C NMR** ($CDCl_3$, 75.5 MHz, 25.0 °C) δ_C 154.3, 146.6, 132.2, 130.2, 127.9, 126.9, 115.1. **UV-Vis** ($CHCl_3$) λ_{max} (nm) 435. **IR** $\bar{\nu}$ (cm^{-1}) 3330 (m, N-H str.).

4,7-Bis(8-(*tert*-butyl)-6*H*,12*H*-5,11-methanodibenzo[*b*,*f*][1,5]diazocin-2-yl)benzo[*c*][1,2,5] thiadiazole (TB-BTZ)

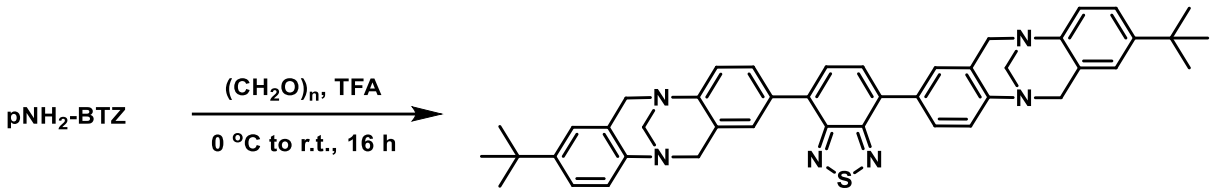

Trifluoroacetic acid (TFA) (10 mL) was cooled with an ice-bath then a mixture of **pNH$_2$-BTZ** (159 mg, 0.5 mmol), *p*-*tert*-butylaniline (1.6 mL, 10 mmol) and paraformaldehyde (630 mg, 21 mmol) added in portions over a 30-minute period. The mixture was warmed to room temperature then stirred for 16 hours under nitrogen. The reaction mixture was poured onto a mixture of 35% NH_3 (aq) (10 mL) diluted with water (100 mL), stirred at room temperature for 2 h then the yellow precipitate obtained by filtration. The crude product was first purified by silica gel column chromatography using acetone:n-hexane 1:2 as the eluent then by reprecipitation from DCM solution onto ice-cold n-hexane to give the final product as a yellow powder (50 mg, 15%). **^{1}H NMR** ($CDCl_3$, 400 MHz, 25.0 °C) δ_H 7.78 (dd, J = 8.4, 1.1 Hz, 2 *H*), 7.64 (s, 2 *H*), 7.51 (d, J = 1.1 Hz, 2 *H*), 7.31 (d, J = 8.4 Hz, 2 *H*), 7.19 (dd, J = 8.5, 2.3 Hz, 2 *H*), 7.08 (d, J = 8.4 Hz, 2 *H*), 6.92 (d, J = 2.1 Hz, 2 *H*), 4.79 (t, J = 17.2 Hz, 4 *H*), 4.40 (s, 4 *H*), 4.28 (d, J = 16.4 Hz, 4 *H*), 1.25 (s, 18 *H*). **^{13}C NMR** ($CDCl_3$, 100 MHz, 25.0 °C) δ_C 154.0, 148.8, 146.9, 145.3, 132.9, 132.5, 128.4, 128.1, 127.7, 127.7, 127.0, 125.3, 124.7, 124.6, 123.5, 66.9, 58.9, 58.6, 34.3, 31.4. **UV-Vis** ($CHCl_3$) λ_{max} (nm) 413. **IR** $\bar{\nu}$ (cm^{-1}) 2958 (m, C-H str.).

PIM-BTZ-5% and PIM-BTZ-1%

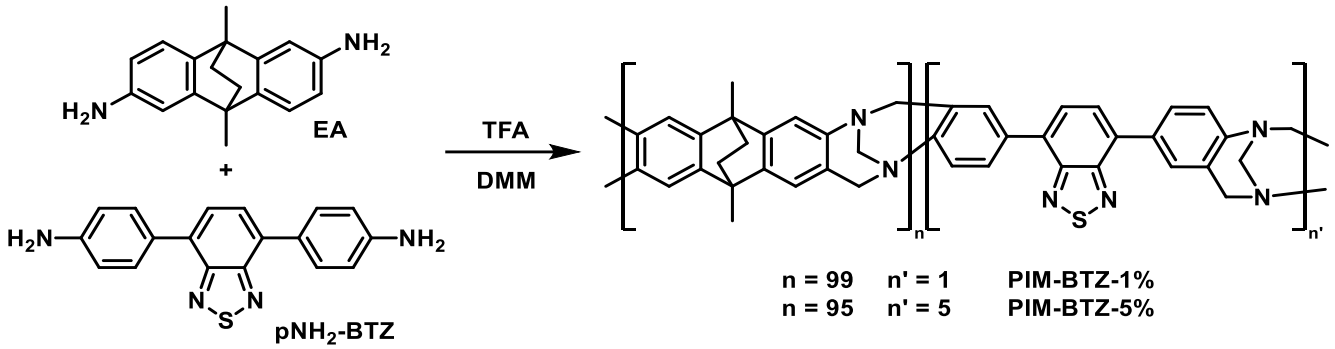

PIM-BTZ-5%

Under a nitrogen atmosphere, **EA** (931 mg, 3.52 mmol) and **pNH$_2$-BTZ** (59 mg, 0.185 mmol) were dissolved in dimethoxymethane (DMM) (1.67 mL, 1.44 g, 18.9 mmol) and cooled with an ice-water bath. Trifluoroacetic acid (TFA) (8.5 mL) was added dropwise over 30-minutes then the reaction mixture was stirred for 48 h at room temperature under nitrogen. After 2 days, the resultant viscous red-orange mixture was poured slowly onto a mixture of aqueous ammonia and ice and stirred vigorously for 2 h. The precipitate was collected by filtration, washed with water and then acetone until all washing were clear. The solid was dissolved in chloroform (35 mL) and methanol was added dropwise until the solution became turbid. The solution was stirred for a further 60 min to precipitate a gel that was obtained by filtration. The re-precipitation from chloroform was repeated twice. The crude polymer was further purified by dissolving in chloroform (30 mL) and the solution added drop-wise to n-hexane (200 ml) with vigorous stirring to precipitate a fine powder. This powder was refluxed in methanol for 48 h, filtered and then dried in a vacuum oven at 100 ^{o}C for 6 h to afford **PIM-BTZ-5%** as a fine yellow powder (673 mg, 67%).

PIM-BTZ-1%

Procedure described above was repeated with **EA** (968 mg, 3.66 mmol) and **pNH$_2$-BTZ** (12 mg, 0.037 mmol) to give **PIM-BTZ-1%** as a light-yellow powder (668 mg, 60%).

3. BTZ Doped PIM-EA-TB Films

Fabrication of BTZ Doped Thin Films

PIM-EA-TB (149 mg) and either **pH-BTZ** (7.2 mg, 25 µmol) or **ThTh-BTZ** (11.5 mg, 25 µmol) were dissolved in $CHCl_3$ (10 mL) then the solution filtered through a Millipore syringe filter directly into a dry circular glass dish with a diameter of 9 cm. The glass dish was then covered, and the solvent evaporated at ambient temperature over 2 days to yield a thin film.

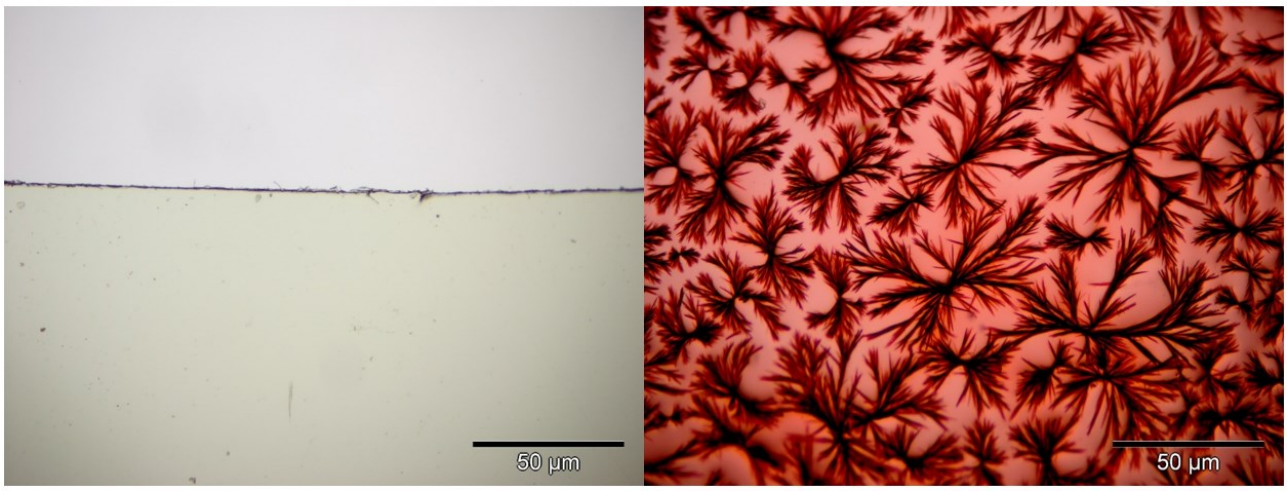

Figure S1 Films of **PIM-EA-TB** with 25 µmol **pH-BTZ** (left) and 25 µmol of **ThTh-BTZ** (right) under an optical microscope.

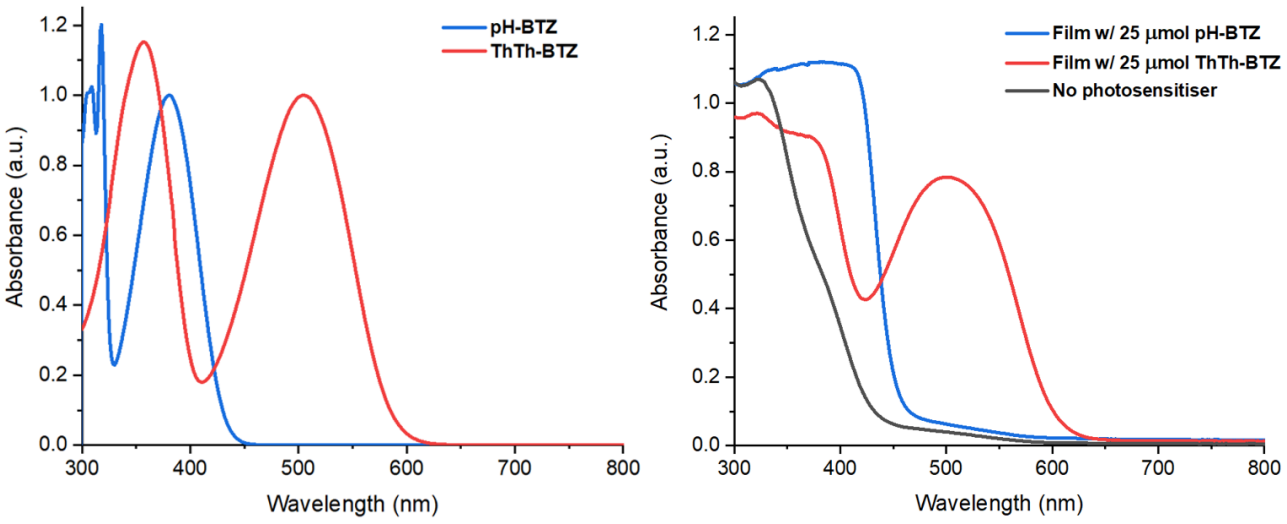

Figure S2 (Left) Normalised UV-Vis absorption spectra of **pH-BTZ** and **ThTh-BTZ** in chloroform solution. (Right) Solid state UV-Vis absorption spectra of **PIM-EA-TB** containing no photosensitiser (grey), 25 µmol **pH-BTZ** (blue) and 25 µmol **ThTh-BTZ** (red).

4. BTZ PIM-EA-TB Copolymers

4.1 Structural Characterisation

Figure S3 Powder samples of **PIM-EA-TB** (A), **PIM-BTZ-1%** (B) and **PIM-BTZ-5%** (C) without (top) and with (bottom) UV-illumination.

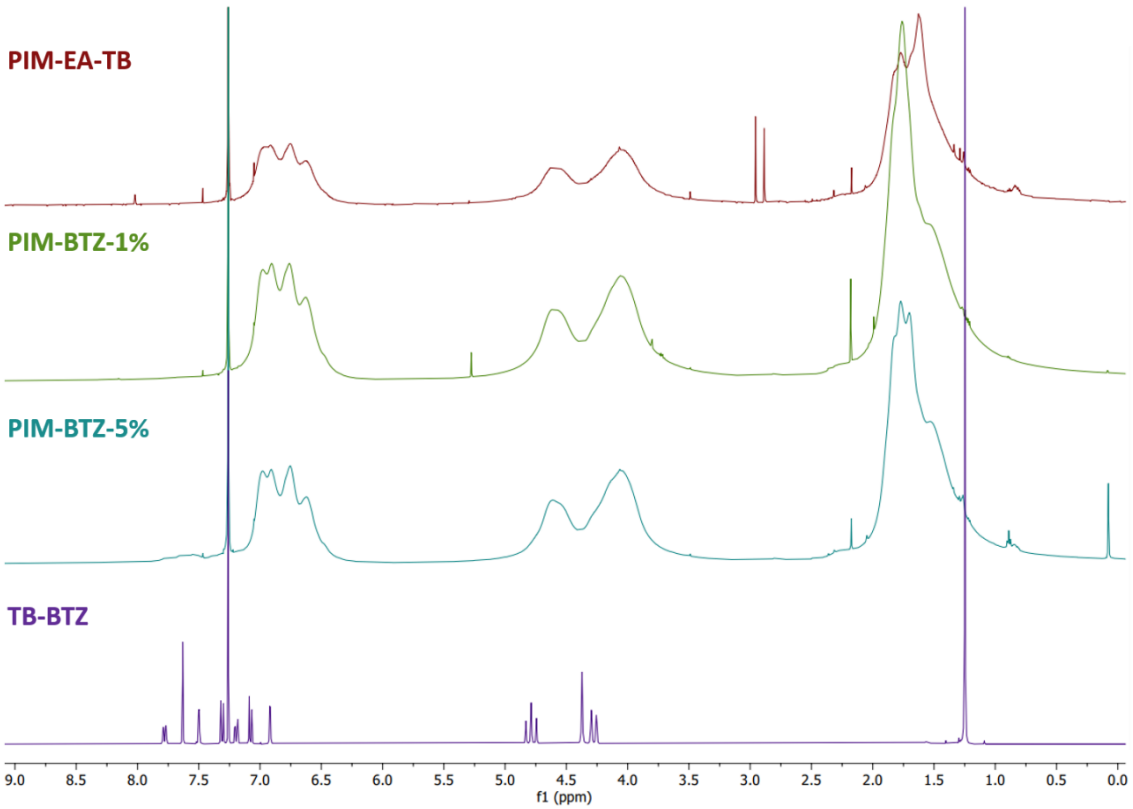

Figure S4 Comparison of the ^{1}H NMR spectra of **PIM-EA-TB** (top), **PIM-BTZ-1%**, **PIM-BTZ-5%**, and **TB-BTZ** (bottom) in $CDCl_3$.

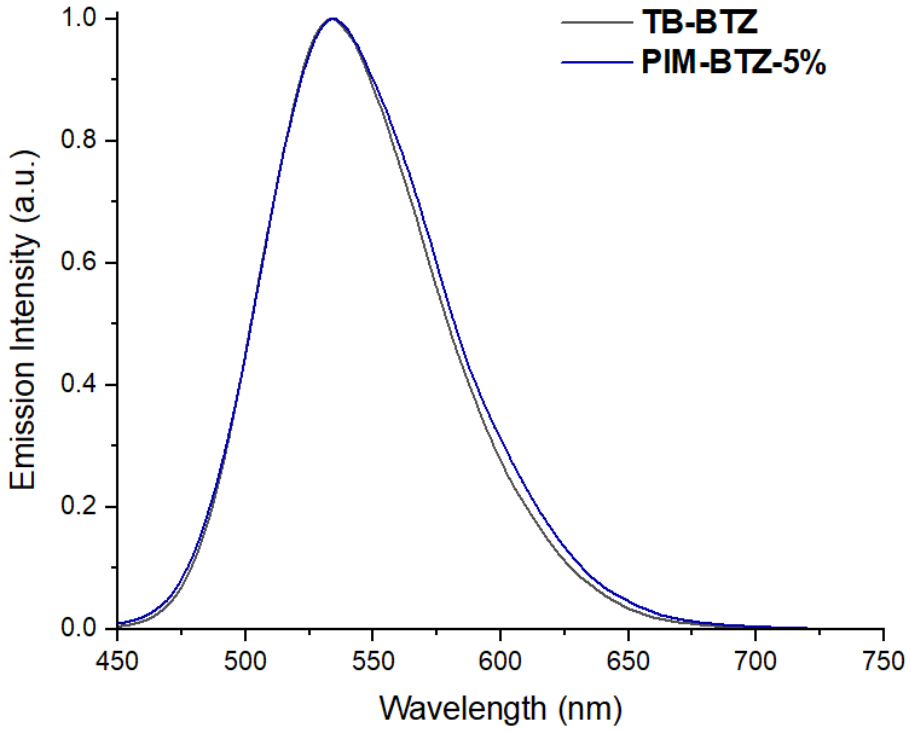

Figure S5 Normalised fluorescence spectra for **PIM-BTZ-5%** and **TB-BTZ** recorded in $CHCl_3$. Excitation wavelength was 412 nm.

Table S1 Solubility studies of **PIM-EA-TB**.[a]

Fully Soluble	**Partial Solubility**	**Insoluble**
Chloroform	Anisole	Acetone
Dichloromethane	Dimethylsulfoxide	Acetonitrile
1,2-Dichloroethane	1,4-Dioxane	Dimethylcarbonate
1,2-Dichlorobenzene	Toluene	Dimethylformamide
N-Methylpyrrolidone		Ethanol
Pyridine		Methanol
Quinoline		Tetrahydrofuran
1,1,2,2-Tetrachloroethane		Water

[a]10 mg of **PIM-EA-TB** + 1 mL of solvent. Mixtures stirred overnight to allow time for dissolution.

Figure S6 Films of **PIM-EA-TB** (left), **PIM-BTZ-1%** (center) and **PIM-BTZ-5%** (right) cast from chloroform solution.

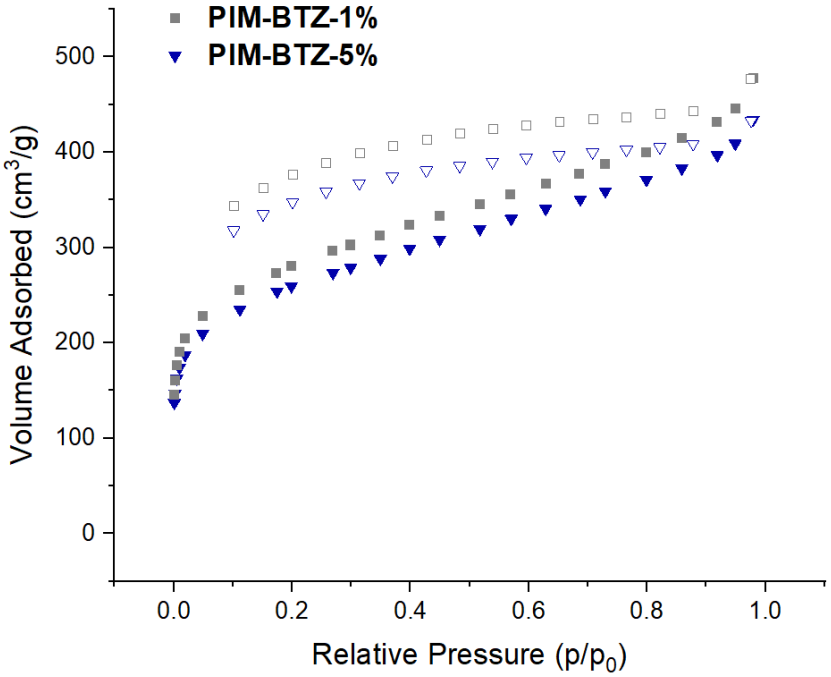

Figure S7 N_2 adsorption (solid) and desorption (hollow) isotherms for **PIM-BTZ-1%** (grey squares) and **PIM-BTZ-5%** (blue triangles) at 77 K.

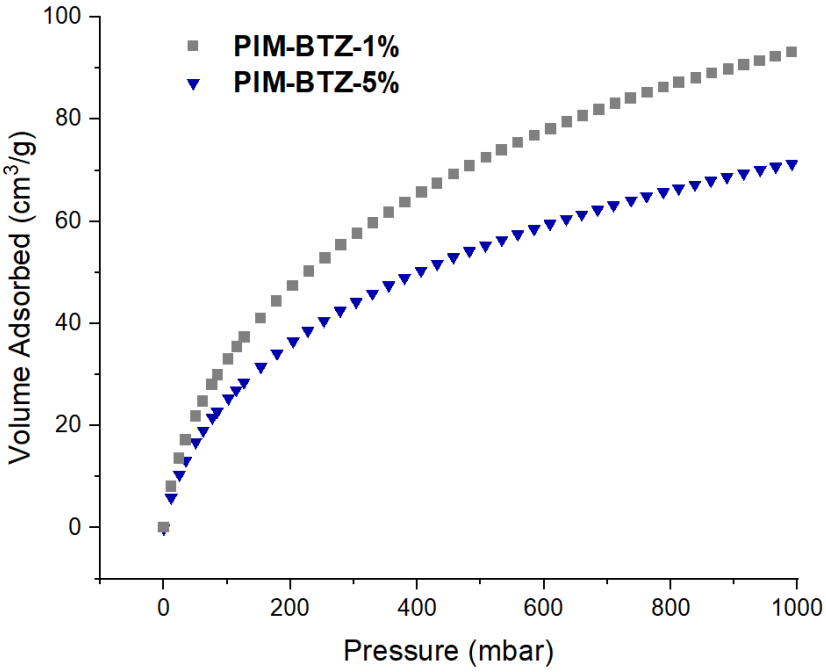

Figure S8 CO_2 adsorption isotherms for **PIM-BTZ-1%** (grey squares) and **PIM-BTZ-5%** (blue triangles) at 273 K.

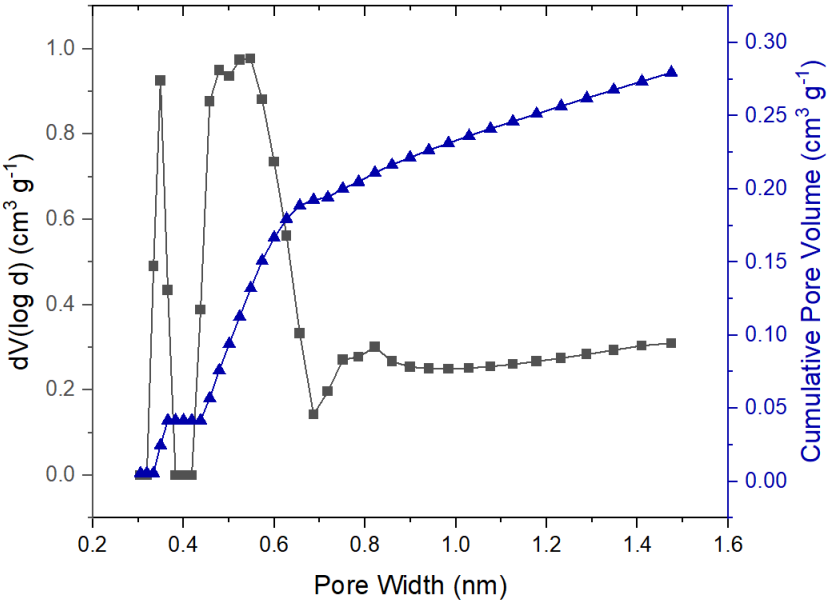

Figure S9 Pore size distribution (grey squares) and cumulative pore volume (blue triangles) for **PIM-BTZ-1%** calculated using NLDFT.

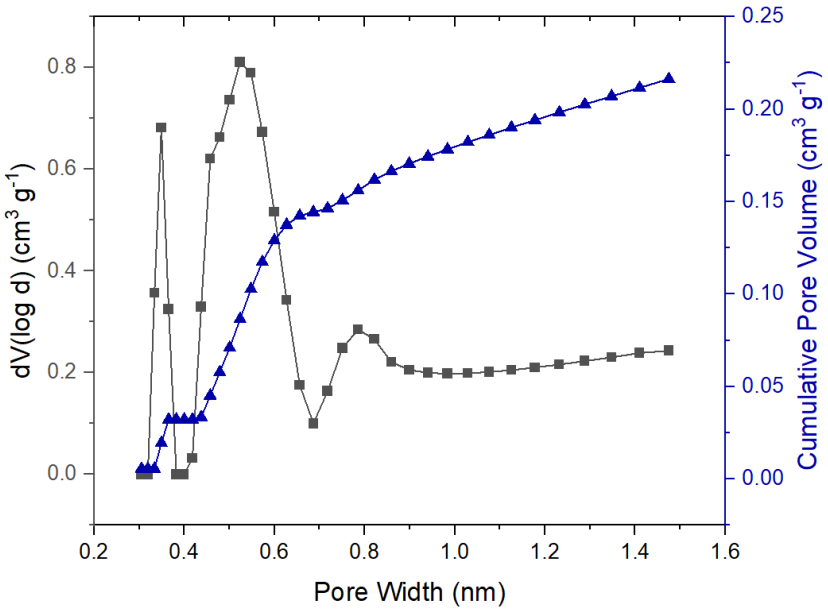

Figure S10 Pore size distribution (grey squares) and cumulative pore volume (blue triangles) for **PIM-BTZ-5%** calculated using NLDFT.

Table S2 Comparison between the BET surface areas of **BTZ** doped **PIM-EA-TB** and select **BTZ** containing porous materials reported in literature.

Material Name	Classification of Material	BET Surface Area ($m^2 g^{-1}$)	Reference
PIM-BTZ-1%	PIM	986	*This work*
PIM-BTZ-5%	PIM	914	*This work*
PIM-EA-TB	PIM	1028	4
PIM-1	PIM	850	5
L-PyBT	Linear Polymer	13	6
P-BT-G41	Crosslinked Polymer Hydrogel	20	7
BCMP-1	Conjugated Porous Polymer	231	8
P-PyBT	Conjugated Porous Polymer	499	6
MOP-1	Microporous Organic Polymer	586	9
Etta-Td	Covalent Organic Framework	749	10
TP-BTD-AA	Covalent Organic Framework	425	11
PCN-57-S	Metal-organic framework	2400	12
JNU-204	Metal-organic framework	805	13

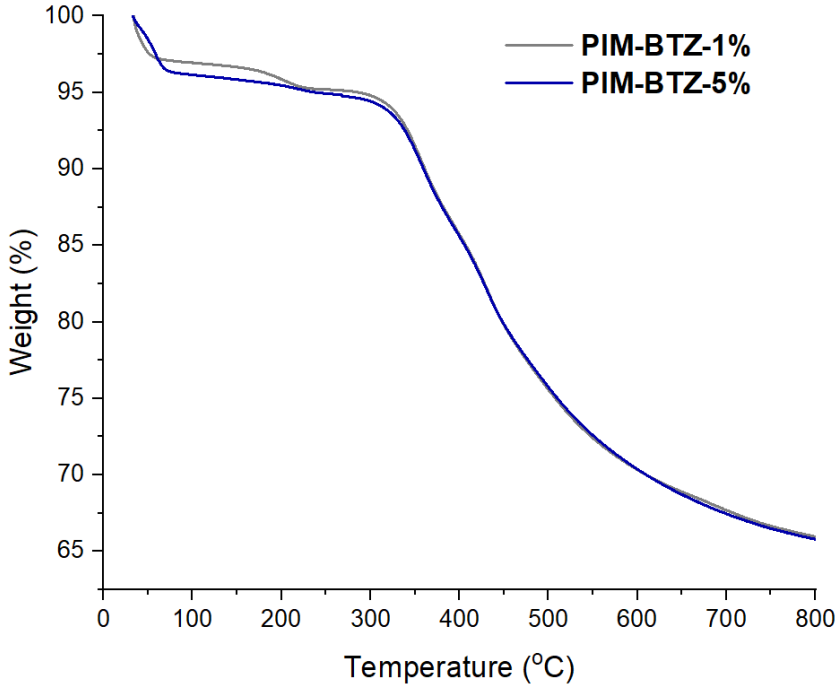

Figure S11 TGA trace for **PIM-BTZ-1%** (grey) and **PIM-BTZ-5%** (blue).

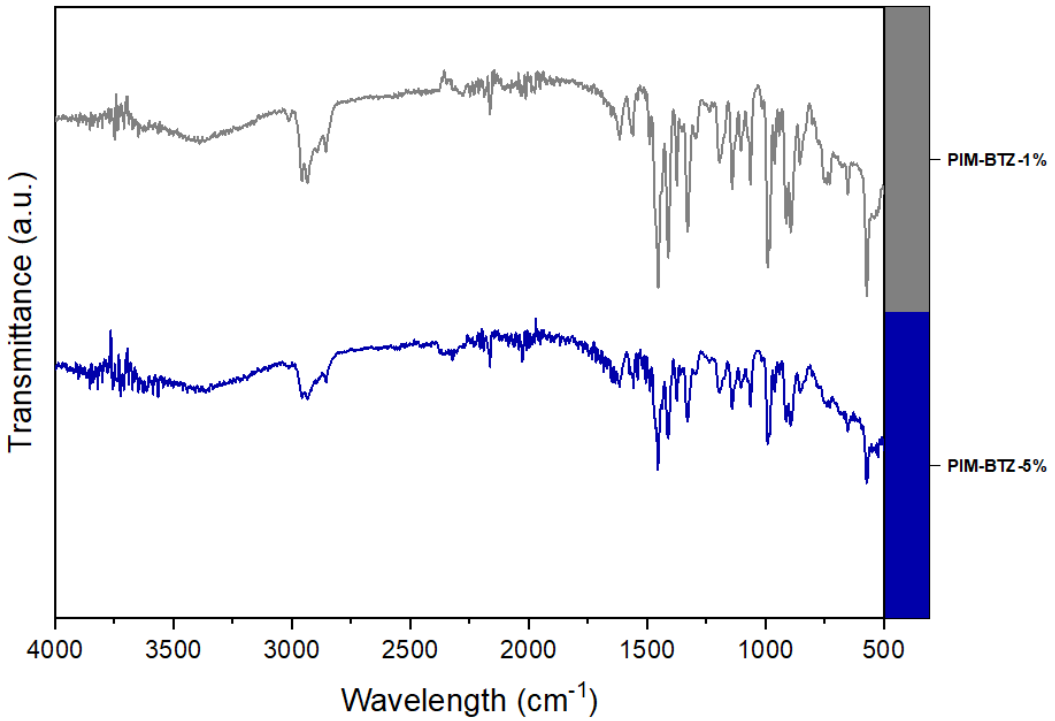

Figure S12 IR spectra for **PIM-BTZ-5%** (blue) and **PIM-BTZ-1%** (grey).

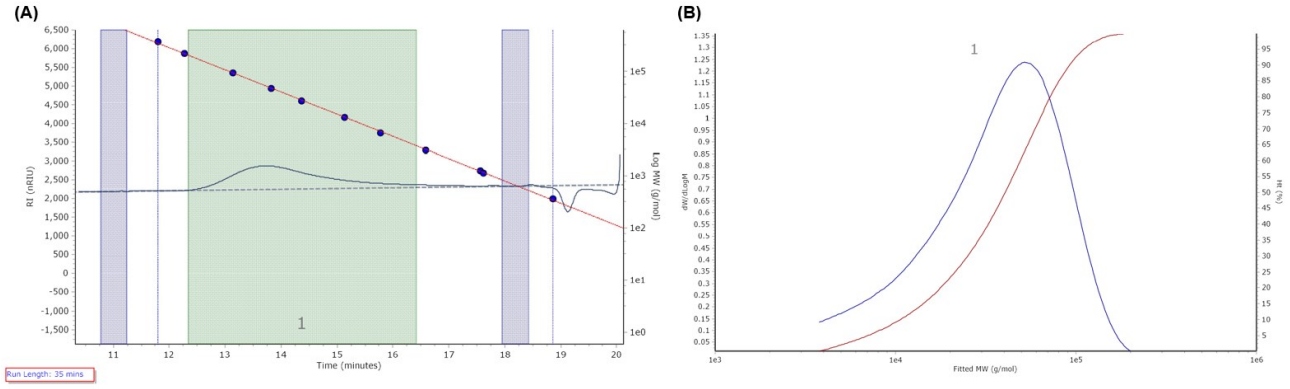

Figure S13 GPC chromatogram (A) and molecular weight distribution (B) for **PIM-EA-BTZ-1%**.

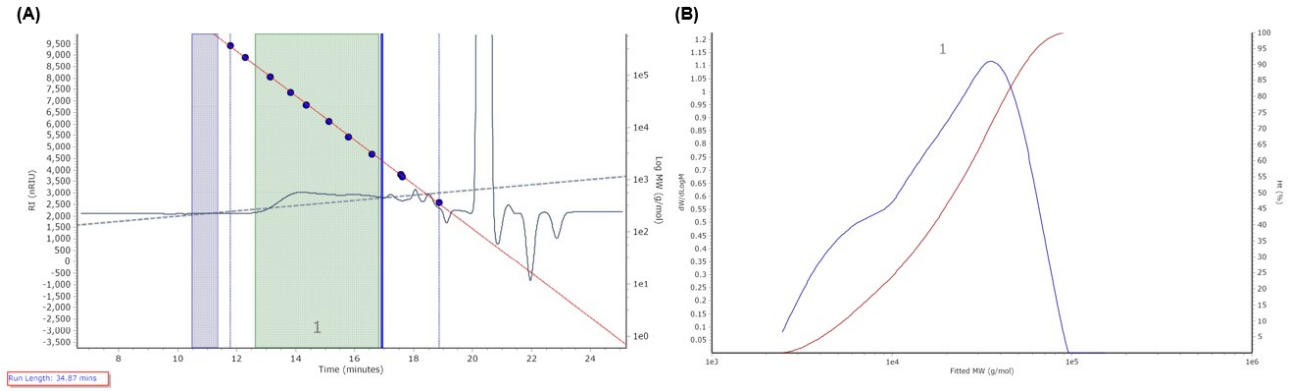

Figure S14 GPC chromatogram (A) and molecular weight distribution (B) for **PIM-EA-BTZ-5%**.

Table S3 Summary of the molecular weights and polydispersity index (PDI) for **PIM-EA-TB**, **PIM-BTZ-1%** and **PIM-BTZ-5%**.

Material	M_n/ g mol^{-1}	M_w/ g mol^{-1}	PDI
PIM-EA-TB[a]	40700	155800	3.83
PIM-BTZ-1%	24229	47002	1.94
PIM-BTZ-5%	13192	26426	2.003

[a]Literature values from reference 4.

4.2 Coating Glass Beads with PIM-BTZ-5%

Procedure for coating glass beads

500 – 750 μm glass beads (5 g) were added to a solution of **PIM-BTZ-5%** (10 mg) dissolved in chloroform (5 mL). The solvent was then removed slowly under reduced pressure until a slurry was formed. The beads were then tipped out onto a large piece of filter paper and spread out to promote drying and prevent clumping. Note, completely removing all the solvent on the rotary evaporator resulted in the beads sticking together.

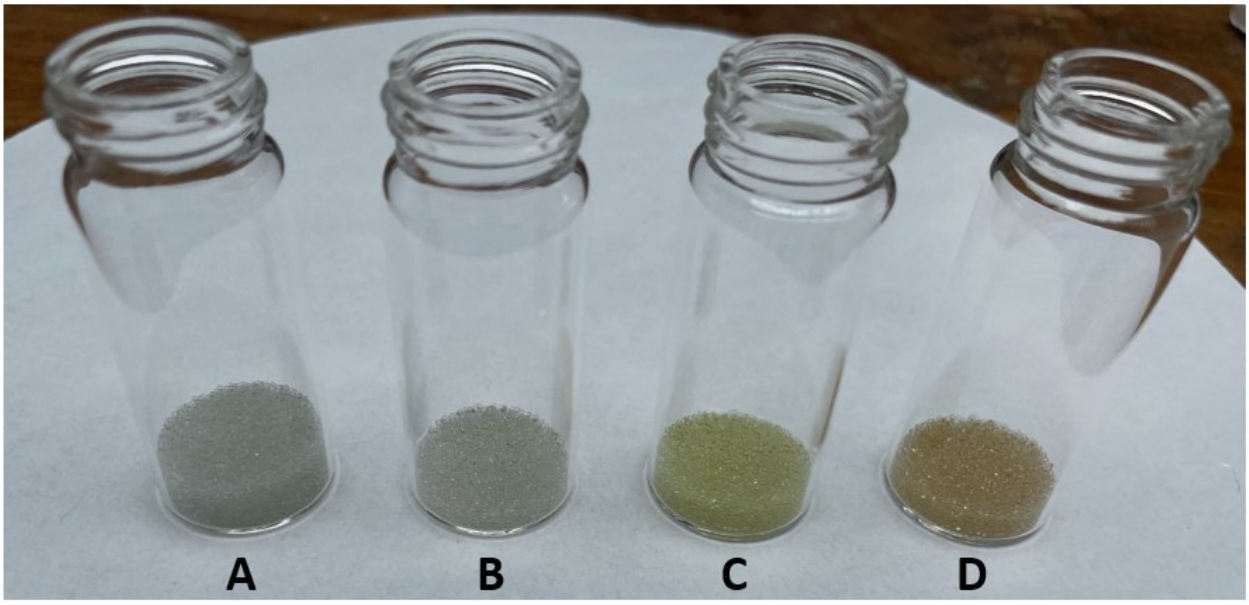

Figure S15 Glass beads without a polymer coating (A), coated with **PIM-EA-TB** (B), coated with **PIM-BTZ-5%** without crosslinks (C) and with crosslinking (D).

Procedure for crosslinking glass beads

Polymer coated glass beads (5 g) were added to a vial then submerged in methanol (5 mL). 1,4-Bis(bromomethyl)benzene (2.6 mg, 0.01 mmol) was added and the mixture heated to 40 °C overnight. The beads were then filtered, washed with methanol then dried under a stream of nitrogen.

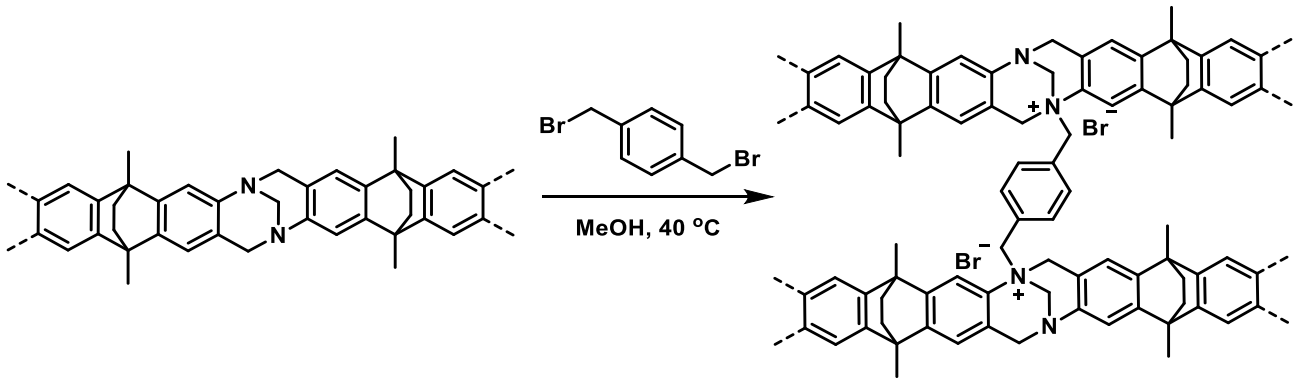

Figure S16 Method for crosslinking **PIM-BTZ-5%** through the Tröger's base linkages.

5. Triarylphosphine Oxidation Reactions

5.1 General Procedure for Triarylphosphine Oxidation

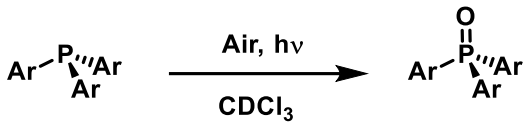

Triarylphosphine (0.20 mmol) and **PIM-BTZ-5%** (10 mg) were added to a vial and dissolved in $CDCl_3$ (5 mL). The mixture was left open to aerate for 10 minutes with stirring then irradiated using a 28 W 420 nm LED. After confirming the reaction was complete by ^{31}P NMR, the reaction mixture was passed through a celite plug followed by DCM (30 mL). The solvent was then removed under reduced pressure to yield the product. NMR spectra agreed with previously published literature.

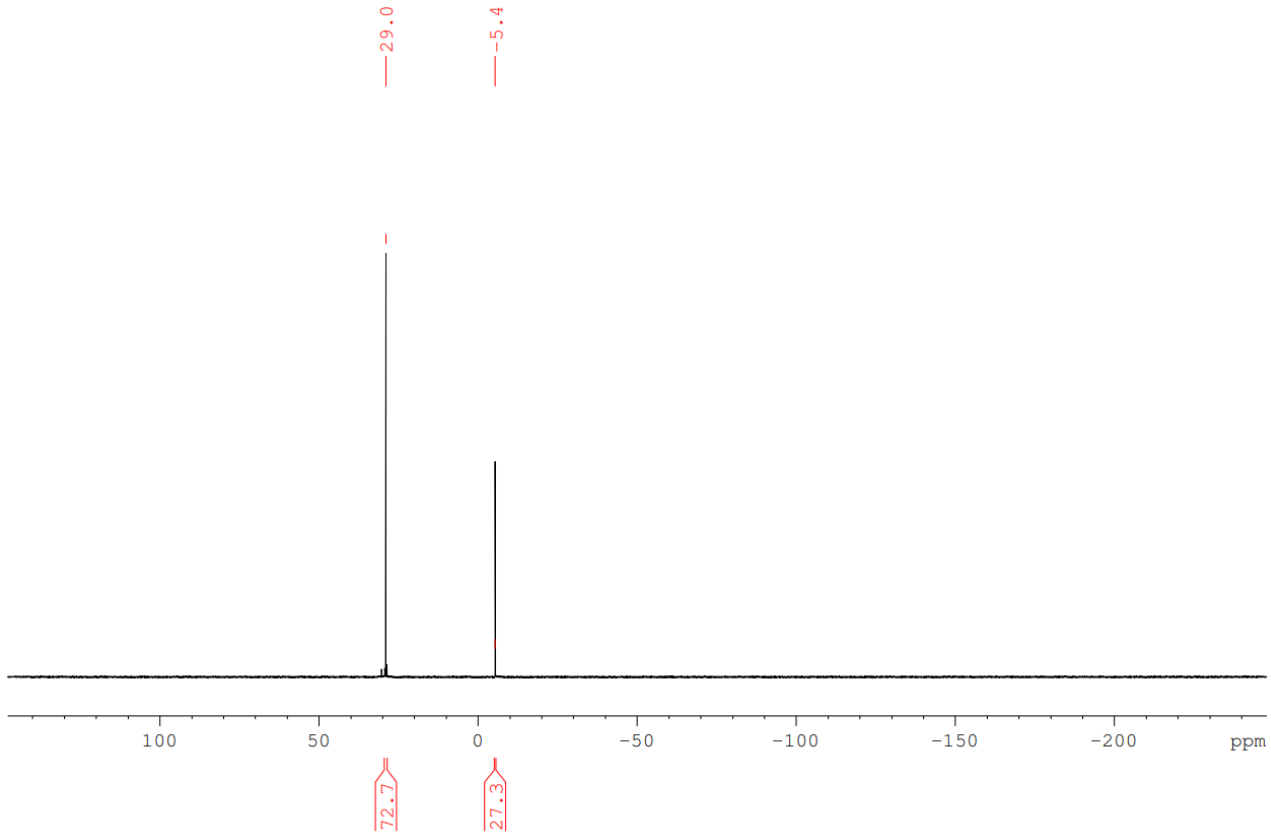

Figure S17 Crude ^{31}P NMR spectra of the PPh_3 oxidation reaction using **TB-BTZ** (NMR conversion – 73%) in $CDCl_3$. Identification of the peaks was made using literature NMR shifts.[16] Triphenylphosphine oxide: 29.0 ppm. Triphenylphosphine oxide: -5.4 ppm.

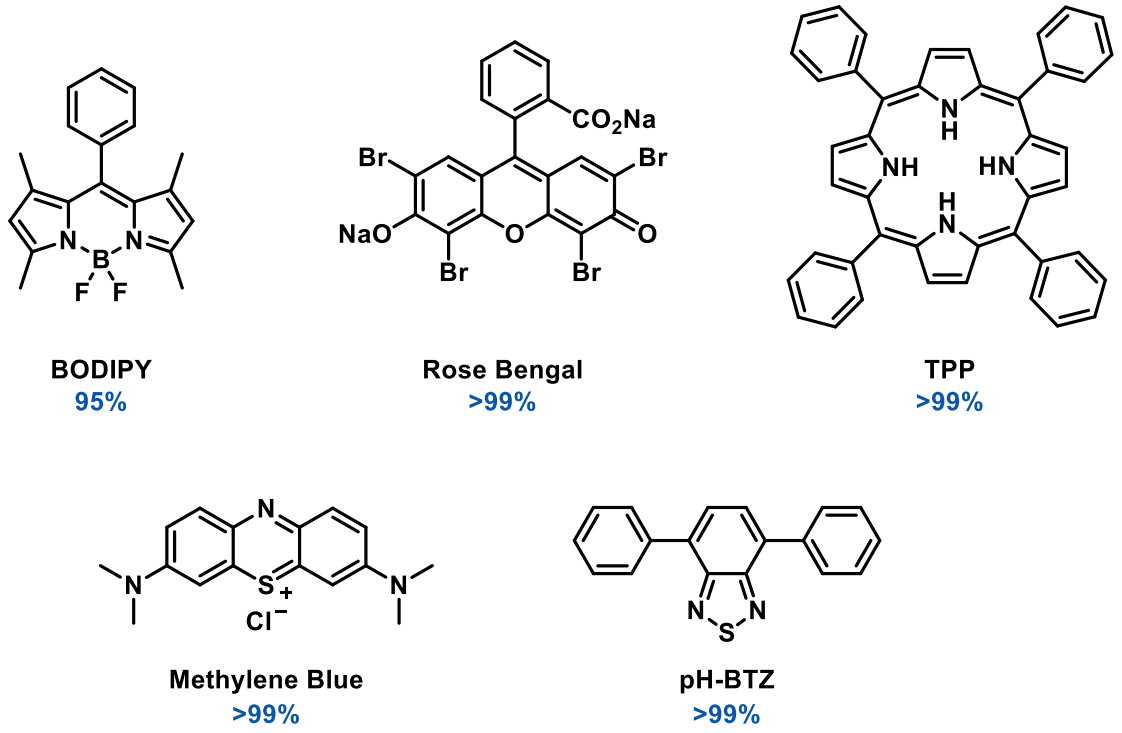

Figure S18 Structure of all benchmark photosensitisers tested in this study. The percentage conversion of triphenylphosphine to triphenylphosphine oxide after 2 hours as measured by ^{31}P NMR spectroscopy is noted. **BODIPY** and **pH-BTZ** were prepared according to literature procedures reported by Vázquez-Romero *et al*. and Taylor *et al*.[3,14] Rose Bengal, tetraphenylporphyrin (TPP) and Methylene Blue were all commercially available. **pH-BTZ** was tested using a 420 nm LED while all other photosensitisers were tested using a daylight white LED light.

5.2 Reaction Scope Characterisation

Triphenylphosphine oxide.[15] Reaction was performed for 6 hours. The product was obtained as off-white crystals (50 mg, 90%). **^{1}H NMR** ($CDCl_3$, 300 MHz, 25.0 °C) δ_H 7.66 (m, 6 *H*), 7.53 (m, 3 *H*), 7.44 (m, 6 *H*). **^{13}C NMR** ($CDCl_3$, 75.5 MHz, 25.0 °C) δ_C 132.6 (d, J = 106.7 Hz), 132.1 (d, J = 10.4 Hz), 131.9 (d, J = 2.9 Hz), 128.5 (d, J = 12.2 Hz). **^{31}P NMR** ($CDCl_3$, 121.5 MHz, 25.0 °C) δ_P 29.0 (m, 1 *P*).

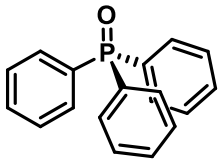

Tri-*p*-tolylphosphine oxide.[15] Reaction was performed for 6 hours. The product was obtained as colourless crystals (55 mg, 87%). **^{1}H NMR** ($CDCl_3$, 300 MHz, 25.0 °C) δ_H 7.53 (dd, 6 *H*, J = 11.7 Hz, 8.1 Hz), 7.25 (dd, 6 *H*, J = 7.9, 2.2 Hz), 2.38 (s, 9 *H*). **^{13}C NMR** ($CDCl_3$, 75.5 MHz, 25.0 °C) δ_C 142.2 (d, J = 2.8 Hz), 132.1 (d, J = 10.1 Hz), 129.7 (d, J = 106.7 Hz), 129.2 (d, J = 12.5 Hz), 21.6 (d, J = 1.0 Hz). **^{31}P NMR** ($CDCl_3$, 121.5 MHz, 25.0 °C) δ_P 29.3 (m, 1 *P*).

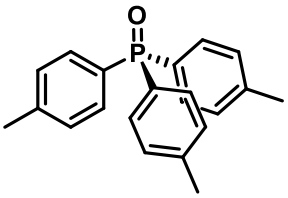

Trimesitylphosphine oxide.[16] Reaction was performed for 18 hours. The product was obtained as a white powder (78 mg, 96%). **^{1}H NMR** ($CDCl_3$, 300 MHz, 25.0 °C) δ_H 6.82 (bs, 6 *H*), 2.17 (m, 27 *H*). **^{13}C NMR** ($CDCl_3$, 75.5 MHz, 25.0 °C) δ_C 140.6 (d, J = 2.7 Hz), 132.8 (s), 131.5 (s), 131.2 (br s), 23.6 (d, J = 4.4 Hz), 21.0 (d, J = 1.4 Hz). **^{31}P NMR** ($CDCl_3$, 121.5 MHz, 25.0 °C) δ_P 29.3 (m, 1 *P*).

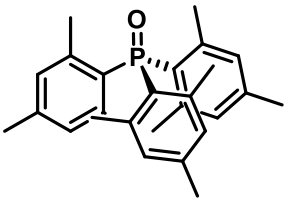

Tris(4-methoxyphenyl)phosphine oxide.[16] Reaction was performed for 6 hours. The product was obtained as a white powder (50 mg, 68%). **^{1}H NMR** ($CDCl_3$, 300 MHz, 25.0 °C) δ_H 7.55 (m, 6 *H*), 6.93 (m, 6 *H*), 3.81 (s, 9 *H*). **^{13}C NMR** ($CDCl_3$, 75.5 MHz, 25.0 °C) δ_C 162.3 (d, J = 2.8 Hz), 133.8 (d, J = 11.2 Hz), 124.5 (d, J = 111.0 Hz), 113.1 (d, J = 13.1 Hz), 55.3 (s). **^{31}P NMR** ($CDCl_3$, 121.5 MHz, 25.0 °C) δ_P 28.7 (m, 1 *P*).

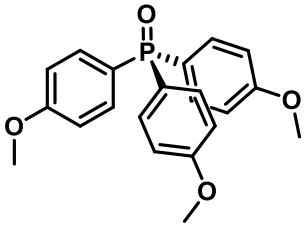

Tris(4-fluorophenyl)phosphine oxide.[15] Reaction was performed for 10 hours. The product was obtained as a white powder (45 mg, 68%). **^{1}H NMR** ($CDCl_3$, 300 MHz, 25.0 °C) δ_H 7.64 (m, 6 *H*), 7.17 (m, 6 *H*). **^{13}C NMR** ($CDCl_3$, 75.5 MHz, 25.0 °C) δ_C 165.2 (dd, J = 254.4, 3.3 Hz), 134.5 (dd, J = 11.5, 8.9 Hz), 128.2 (dd, J = 108.3, 3.4 Hz), 116.1 (dd, J = 21.5, 13.4 Hz). **^{19}F NMR** ($CDCl_3$, 282.2 MHz, 25.0 °C) δ_F -106.0 (m, 3 *F*). **^{31}P NMR** ($CDCl_3$, 121.5 MHz, 25.0 °C) δ_P 26.8 (m, 1 *P*).

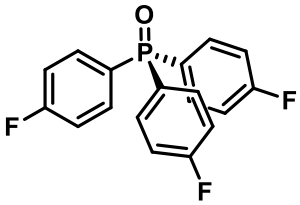

5.3 PIM-BTZ-5% Recycling Experiments

Triphenylphosphine (52 mg, 0.20 mmol) and **PIM-BTZ-5%** (10 mg) were added to a vial and dissolved in acetonitrile (5 mL). The mixture was left open to aerate for 10 minutes with stirring then irradiated using a 28 W 420 nm LED for 12 hours. The reaction mixture was centrifuged at 300 rpm for 5 minutes then the supernatant decanted off and retained. The solid residue was washed with acetonitrile (7 x 5 mL). With each acetonitrile wash, the reaction mixture was mechanically agitated with a laboratory shaker, centrifuged at 300 rpm for 5 minutes and the supernatant decanted off. All the acetonitrile fractions were collected, evaporated under reduced pressure then dissolved in $CDCl_3$ for analysis by ^{1}H and ^{31}P NMR spectroscopy. The residual PIM powder was transferred to a fresh vial for repeating the experiment with additional triphenylphosphine (52 mg) for a total of five runs.

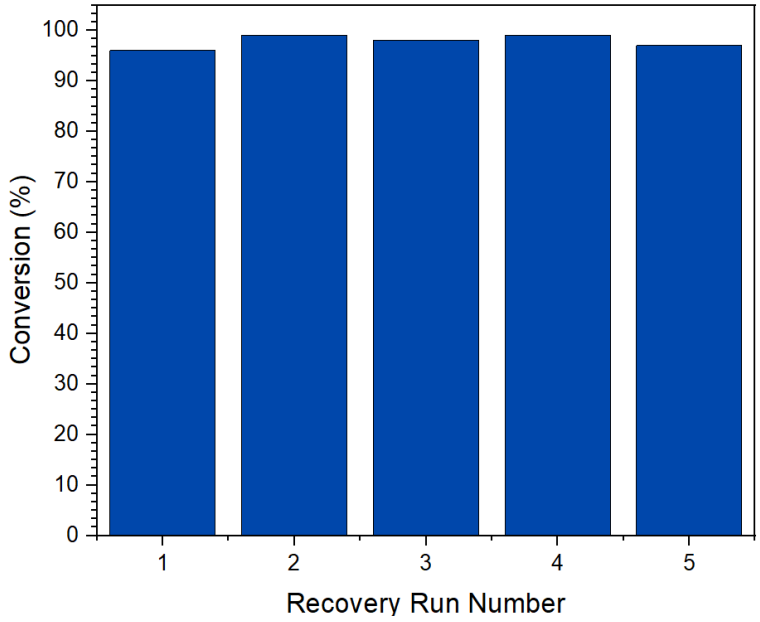

Figure S19 Reusability of **PIM-BTZ-5%** in triphenylphosphine oxidation across five experiments.

5.4 Continuous Flow Photosensitisation Using PIM-BTZ-5% in Solution

Example procedure for triarylphosphine oxidation under continuous flow conditions

Triphenylphosphine (52 mg, 0.2 mmol), **PIM-BTZ-5%** (10 mg) and $CDCl_3$ (5 mL) were added to a glass vial then this mixture was then pumped using a peristaltic pump (pump A) through a 5 mL coil of transparent tubing at a flow rate of 1 mL min^{-1}. Concurrently, air directly from the atmosphere was pumped through a second pump (pump B) at 1 mL min^{-1}, meeting the reaction mixture stream at a T-piece to produce a segmented flow through the reactor. The 5 mL reactor coil was irradiated with a 28 W 420 nm LED for 1 hr then a sample withdrawn for analysis by ^{31}P NMR spectroscopy.

Table S4 Optimisation of triphenylphosphine oxidation under continuous flow conditions.

Entry[a]	Reaction Mixture Flow Rate/ mL min^{-1}	Air Flow Rate/ mL min^{-1}	Reaction Time/ h	Conversion/ %[b]
1	1.0	1.0	1	69
2	1.0	0.5	1	93
3	1.0	2.0	1	55
4	1.0	0.0	1	65
5	2.0	1.0	1	85
6	0.5	1.0	1	46

[a]0.2 mmol PPh_3, 10 mg **PIM-BTZ-5%**, $CDCl_3$. [b]Analysed by ^{31}P NMR spectroscopy.

5.5 Continuous Flow Photosensitisation Using PIM-BTZ-5% Coated Glass Beads

Example procedure for triarylphosphine oxidation under continuous flow conditions

A solution of triphenylphosphine (52 mg, 0.2 mmol) in $CDCl_3$ (5 mL) was pumped using a peristaltic pump (pump A) through a fritted glass column packed with PIM coated glass beads (5 g) at a flow rate of 1 mL min^{-1}. Concurrently, air directly from the atmosphere was pumped through a second pump (pump B) at 1 mL min^{-1} meeting the reaction mixture stream at a T-piece, producing a segmented flow through a fritted glass column containing 5 g of **PIM-BTZ-5%** coated glass beads.

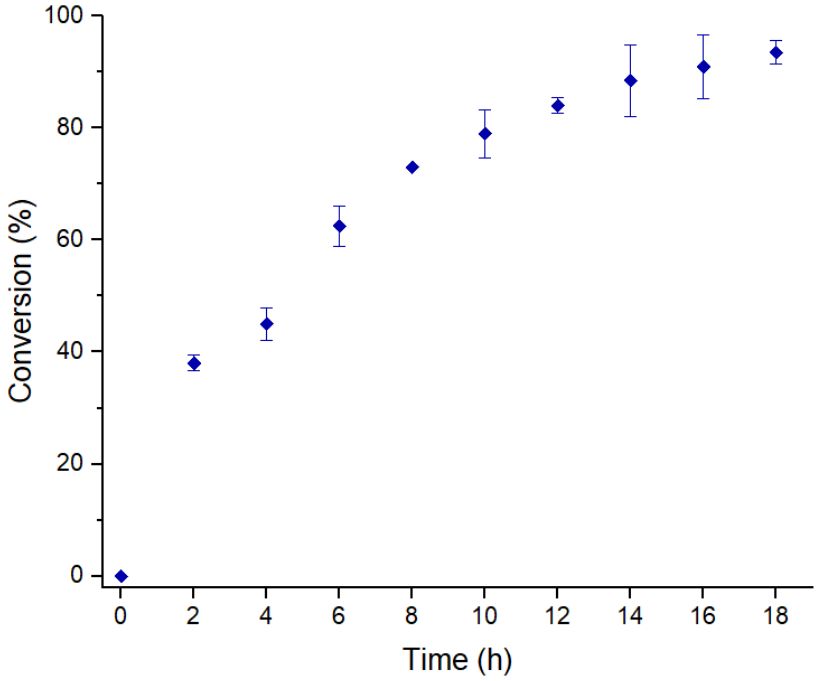

Figure S20 Kinetic trace for the oxidation of triphenylphosphine to triphenylphosphine oxide. Data is the average of three runs with fresh beads in each reactions with standard deviation as the error.

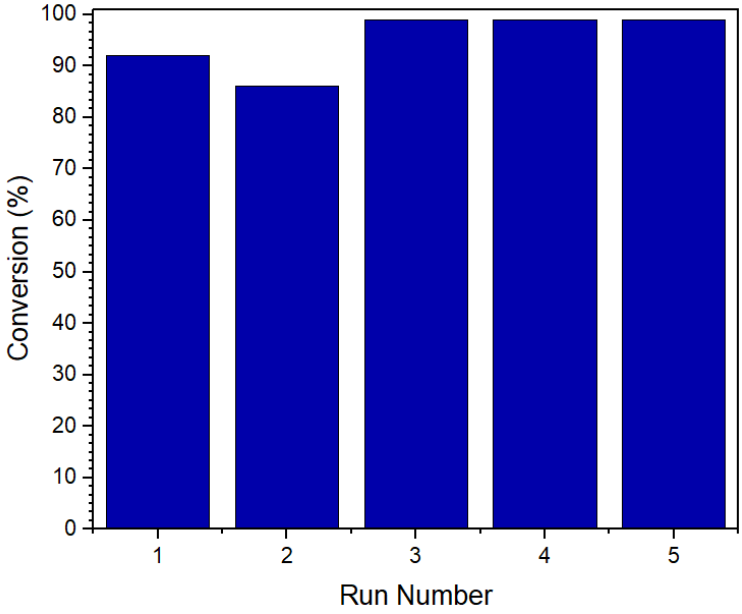

Figure S21 Reusability of glass beads coated with **PIM-BTZ-5%** in triphenylphosphine oxidation across five experiments.

Oxidation of 2-Furoic Acid Using BTZ Doped PIM-EA-TB Films

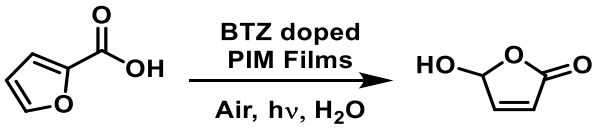

PIM-EA-TB (29.8 mg) and **pH-BTZ** (1.4 mg, 0.005 mmol) were added to an oven dried vial and chloroform (2 mL) added. The mixture was sonicated to ensure complete dissolution then the solvent was allowed to evaporate over 2 days to yield a thin film on the bottom of the vial. Furoic acid (56 mg, 0.5 mmol) and deionised water (5 mL) were added then the mixture irradiated using a 28 W 420 nm LED, without stirring the mixture. After 7 days, a sample was withdrawn from the vial then diluted in D_2O (H_2O:D_2O v/v 9:1) for analysis by ^1H NMR spectroscopy using chemical shifts for starting material and product previously reported in literature.[17]

6. Computational Calculations

All time-dependent (TD)[18] density functional theory calculations (DFT)[19,20] were performed with Gaussian 16 Rev. C.02.[21] The ground state geometry (S_0) of **TB-BTZ** was computed using the B3LYP[22–24] exchange-correlation functional with all other calculations using the long-range corrected CAM-B3LYP functional.[25] An external reaction field matching chloroform, SMD model,[26] was used in all calculations along with the cc-pVTZ basis set.[27,28] This computational setup has been shown to accurately describe similar substituted BTZ systems.[3,29] When applicable, geometries were validated to be minimum energy arrangements at the chosen level of theory through computation of the Hessian matrix ensuring all modes had positive curvature. The predicted absorption spectrum provided in Figure S21 contained 50 singlet states (S_1-S_{50}) and was generated using Gaussian functions centred on the excitation energy, having a full width at half maximum of approximately 50 nm. The lowest triplet state (T_1) state was modelled as a linear response to a singlet ground state reference, *i.e.* using TD-DFT, employing the Tamm-Dancoff approximation.[30]

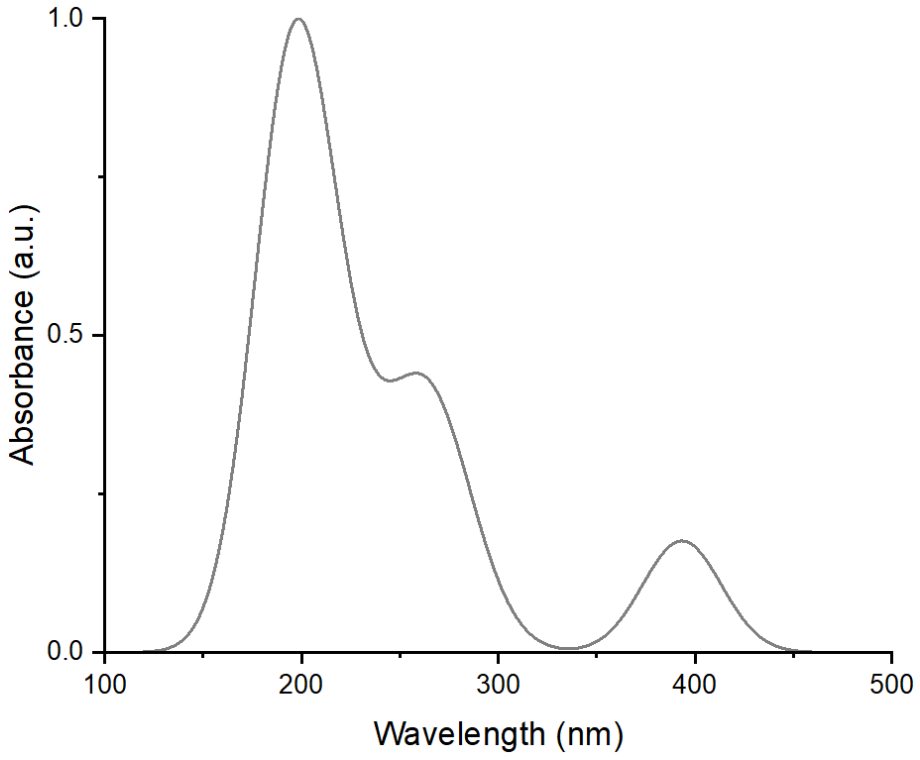

Figure S22 Normalised theoretical UV-Vis spectra of **TB-BTZ**.

Table S5 Summary of calculated properties for **TB-BTZ**. The vertical energies are computed using the same geometries, either the S_0 or T_1 optimal geometry, for the $S_0 \rightarrow S_1$ or $S_0 \rightarrow T_1$ transition, respectively, whereas adiabatic energies are computed at the optimal geometries for each of the electronic states.

	Vertical $S_0 \rightarrow S_1$ / eV	**Osc. Strength**	**Adiabatic $S_0 \rightarrow S_1$/ eV**	**Adiabatic $S_0 \rightarrow T_1$ / eV**	**Vertical $S_0 \rightarrow T_1$ / eV**
TB-BTZ	3.15	0.5501	2.66	1.80	1.38

7. Characterisation Data

Di-*tert*-butyl-(benzo[*c*][1,2,5]thiadiazole-4,7-diylbis(4,1-phenylene))dicarbamate

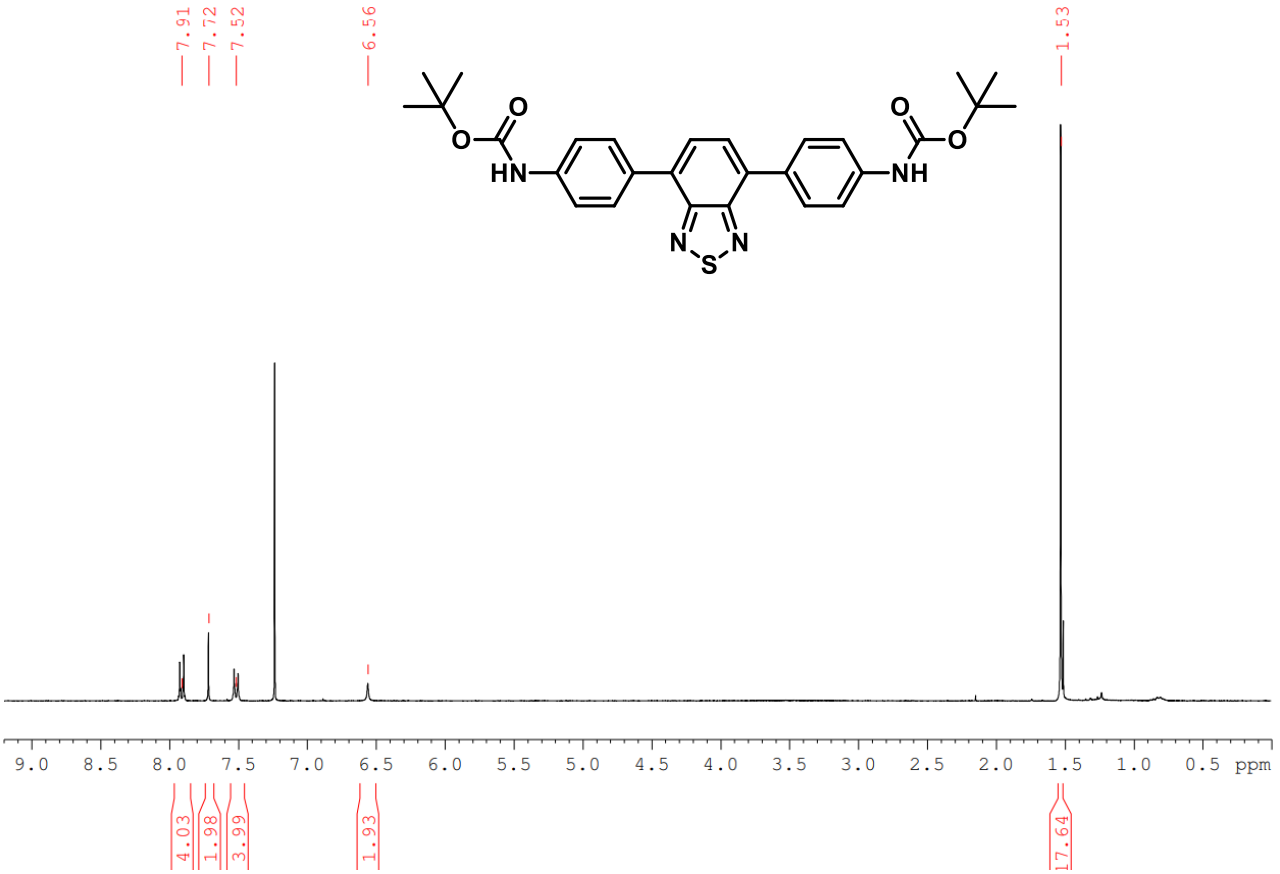

Figure S23 ^{1}H NMR spectra of **pNHBoc-BTZ** in $CDCl_3$.

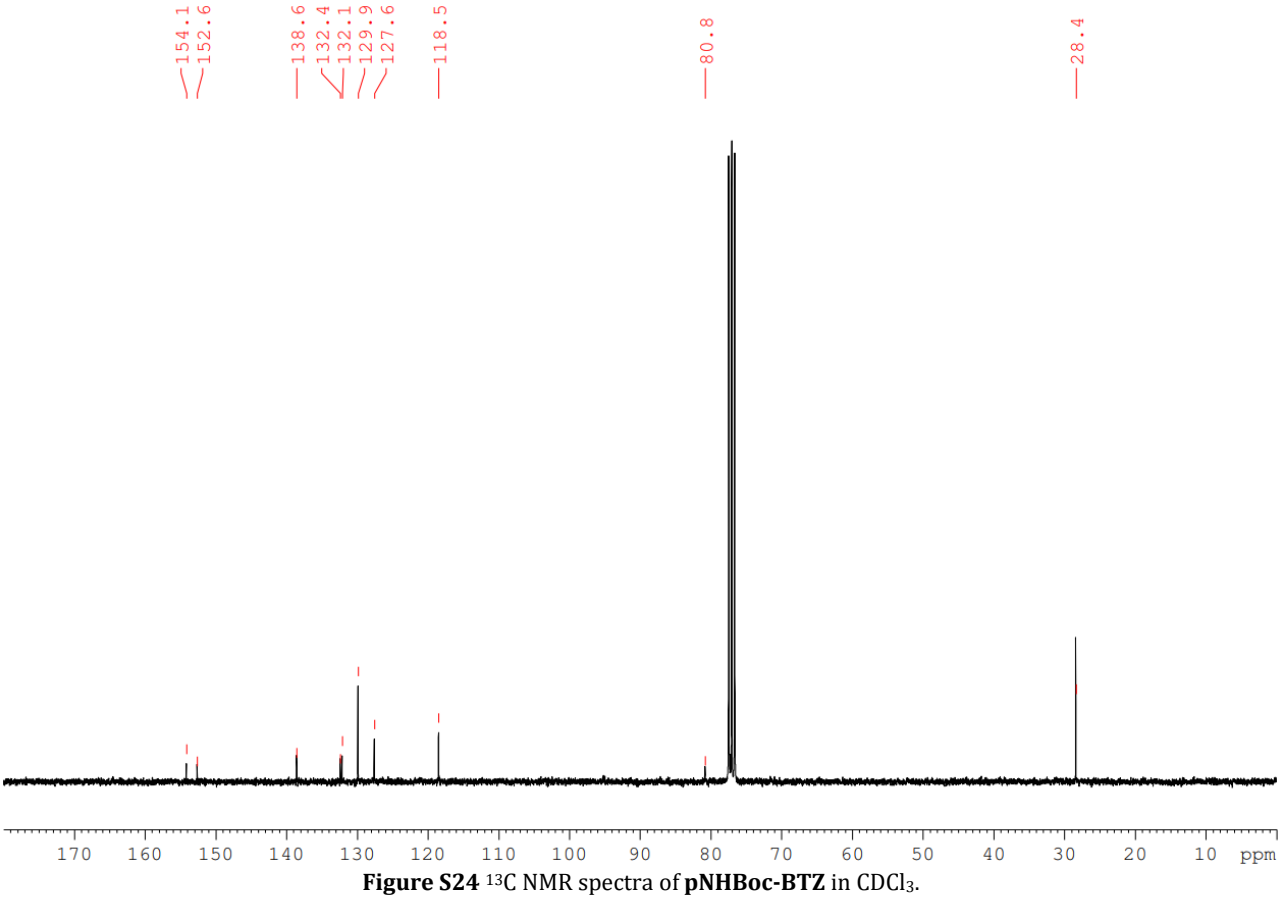

Figure S24 ^{13}C NMR spectra of **pNHBoc-BTZ** in $CDCl_3$.

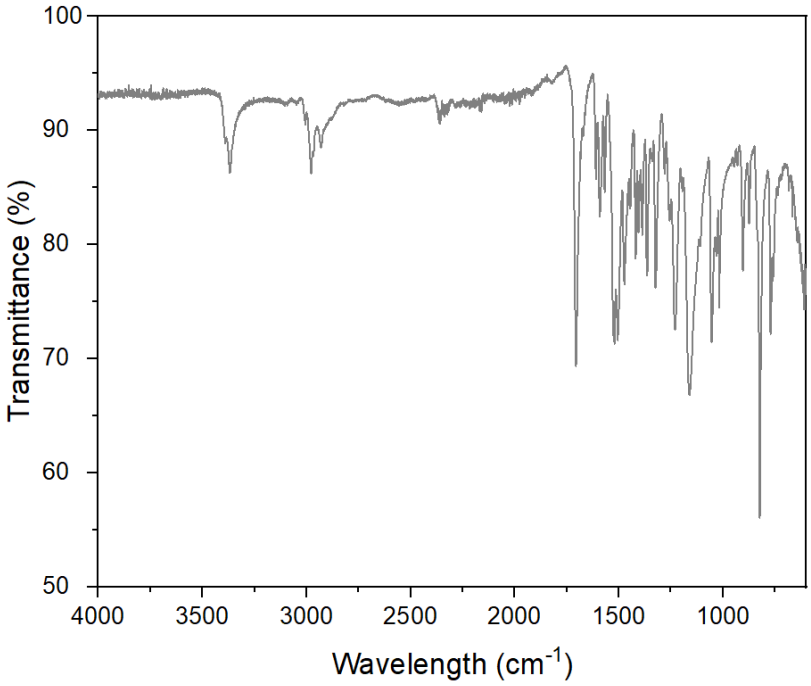

Figure S25 IR spectra of **pNHBoc-BTZ**.

4,4'-(Benzo[*c*][1,2,5]thiadiazole-4,7-diyl)dianiline

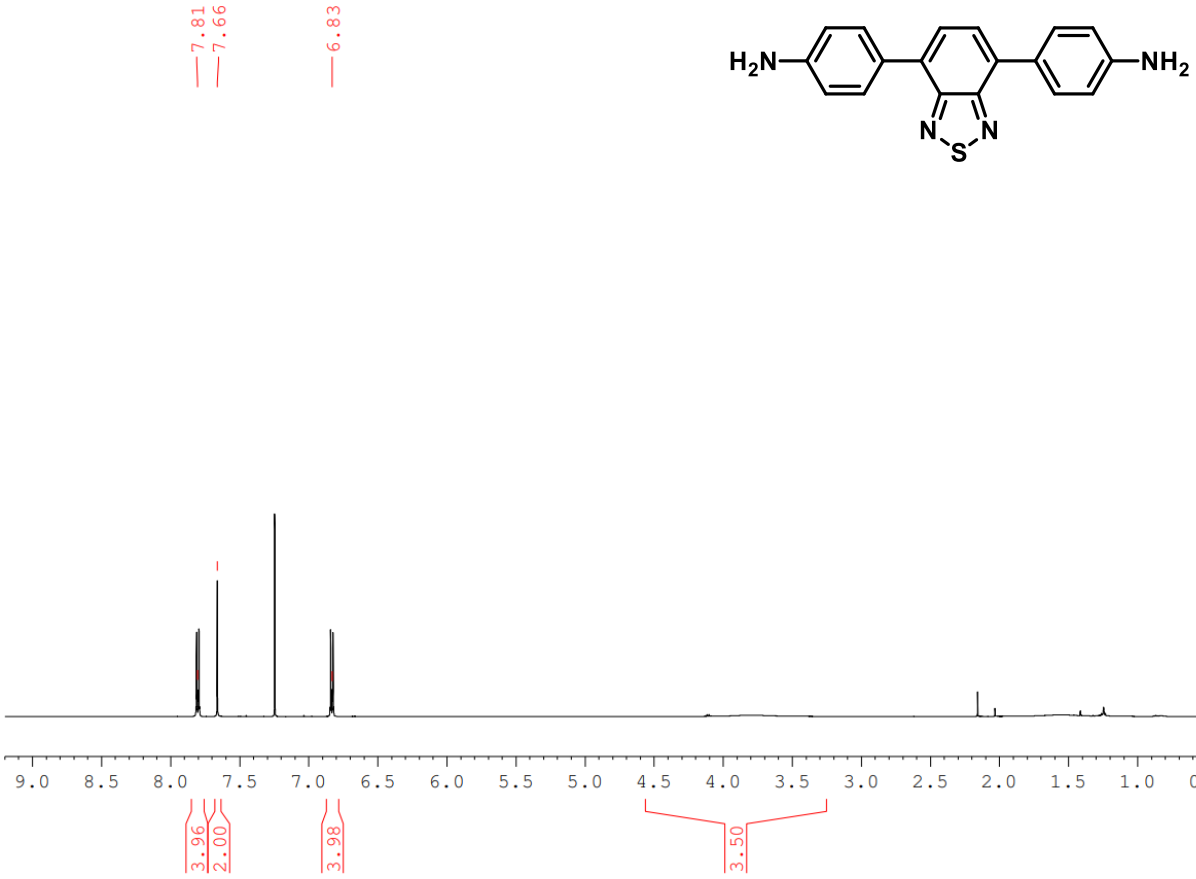

Figure S26 ^{1}H NMR spectra of **pNH$_2$-BTZ** in CDCl$_3$.

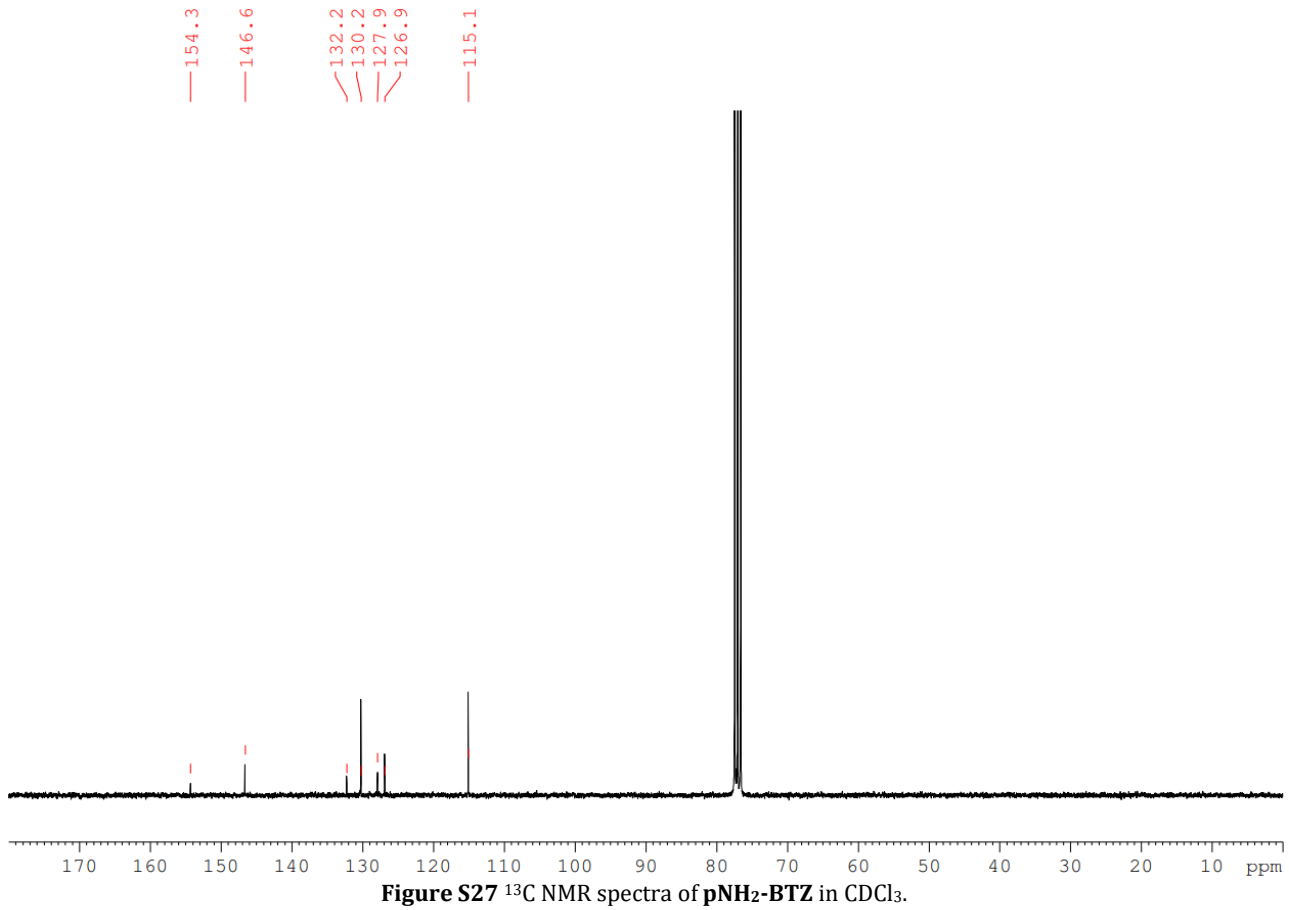

Figure S27 ^{13}C NMR spectra of **pNH$_2$-BTZ** in CDCl$_3$.

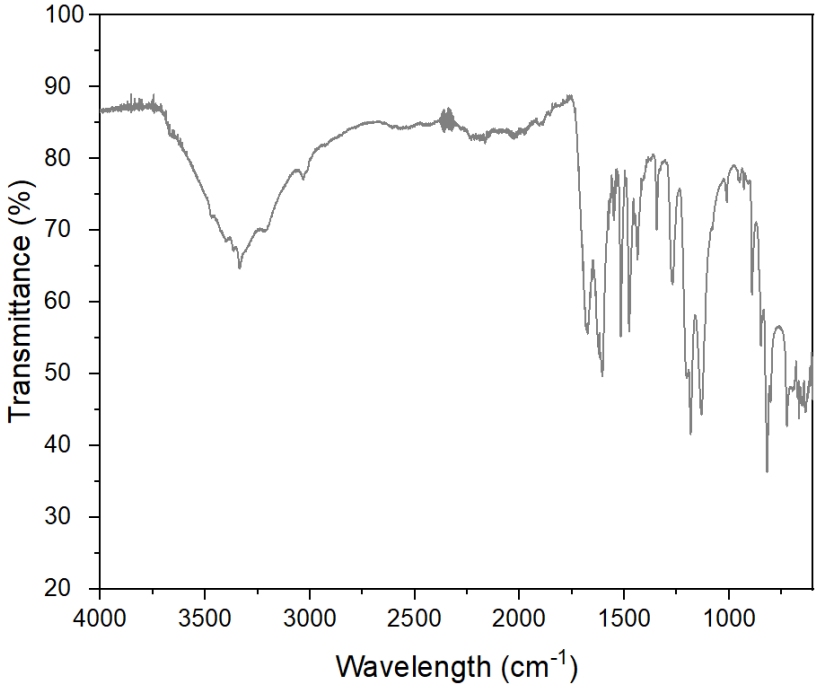

Figure S28 IR spectra of **pNH$_2$-BTZ**.

PIM-BTZ-5%

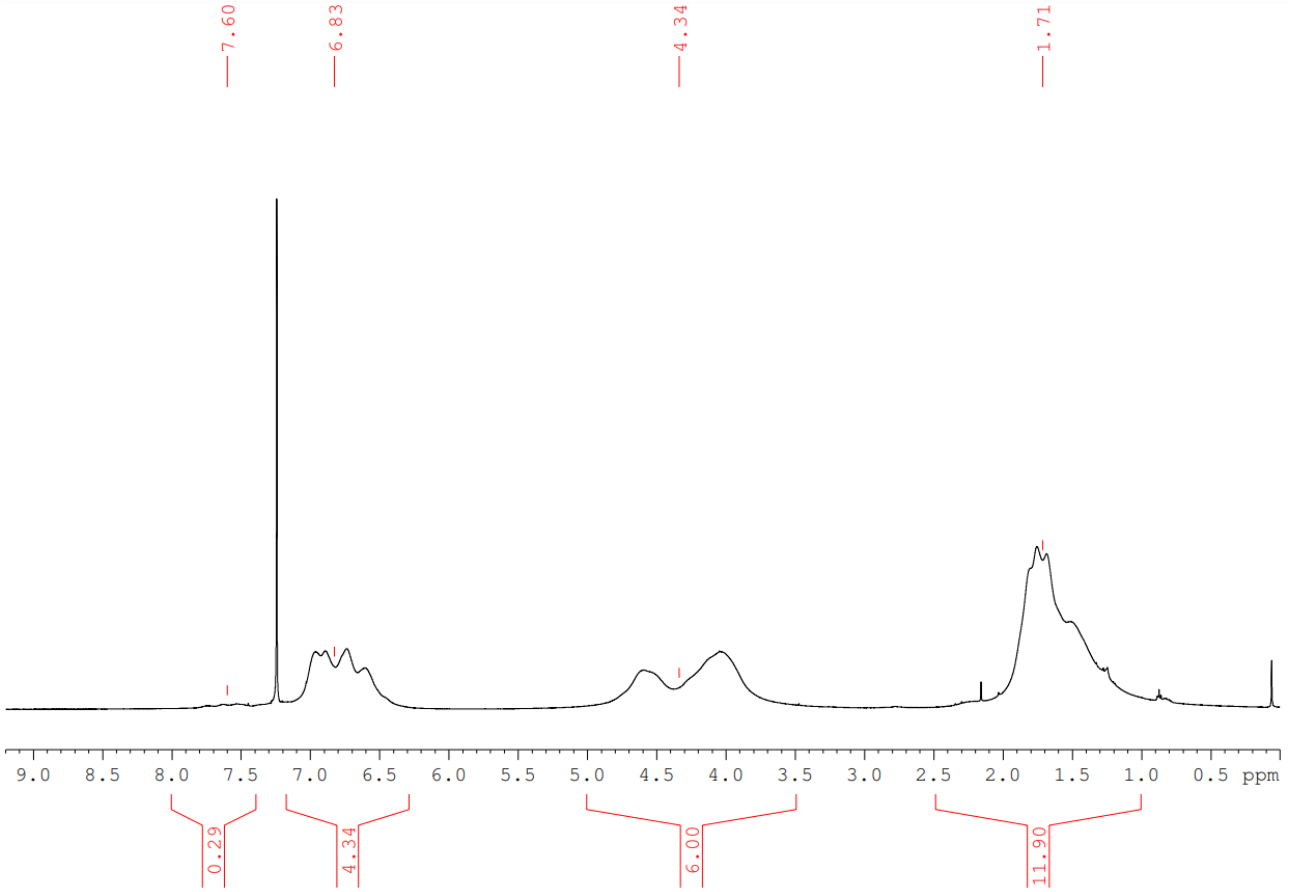

Figure S29 ^{1}H NMR spectra of **PIM-BTZ-5%** in $CDCl_3$.

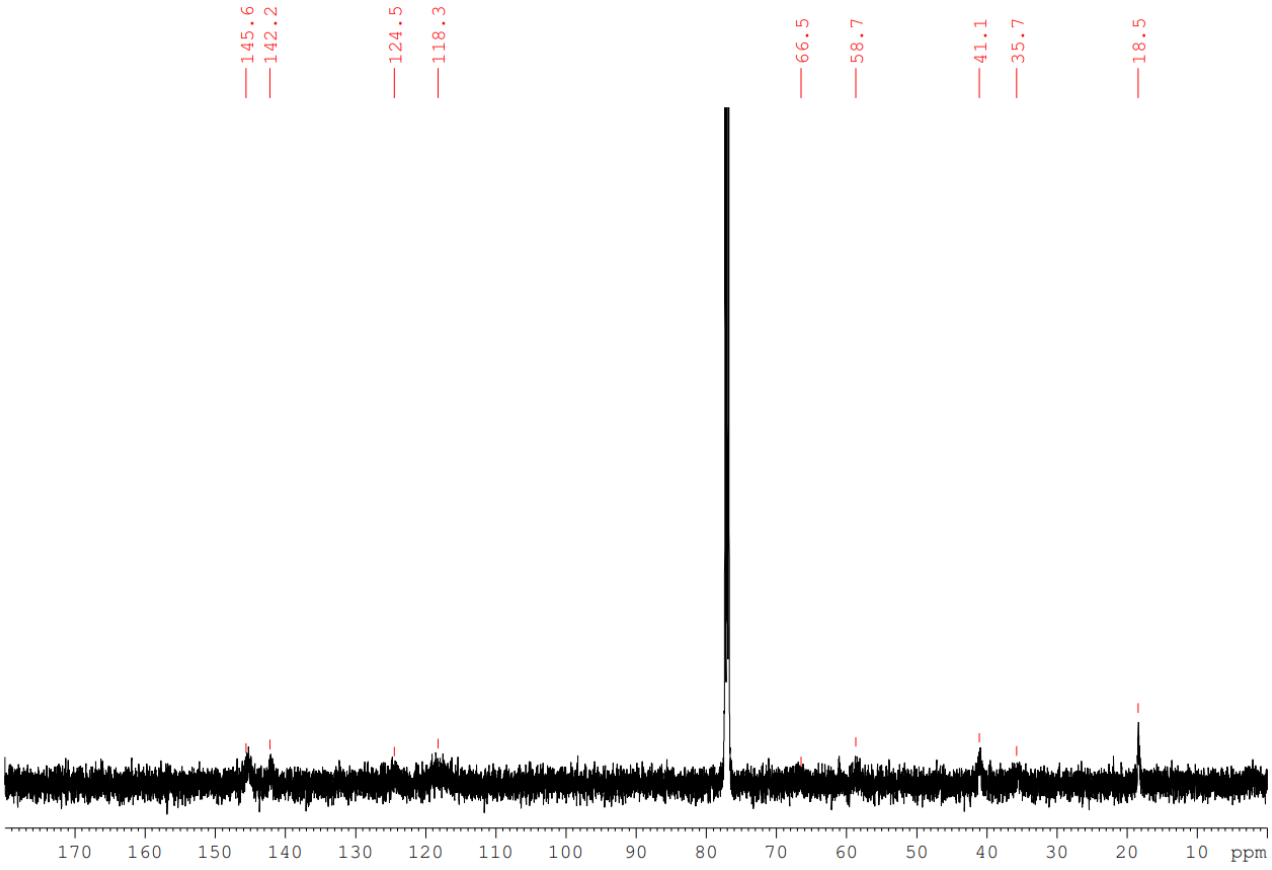

Figure S30 ^{13}C NMR spectra of **PIM-BTZ-5%** in $CDCl_3$.

PIM-BTZ-1%

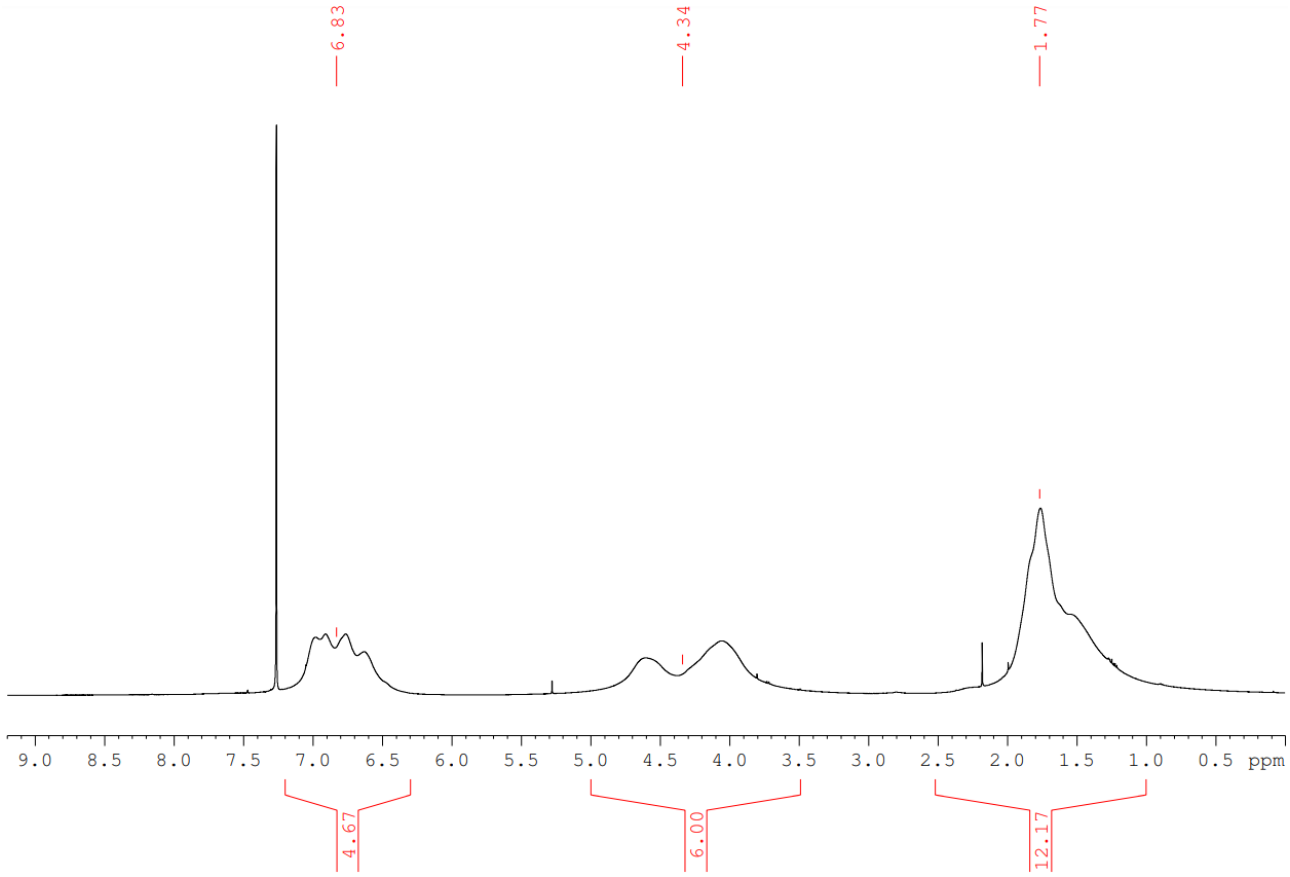

Figure S31 ^{1}H NMR spectra of **PIM-BTZ-1%** in $CDCl_3$.

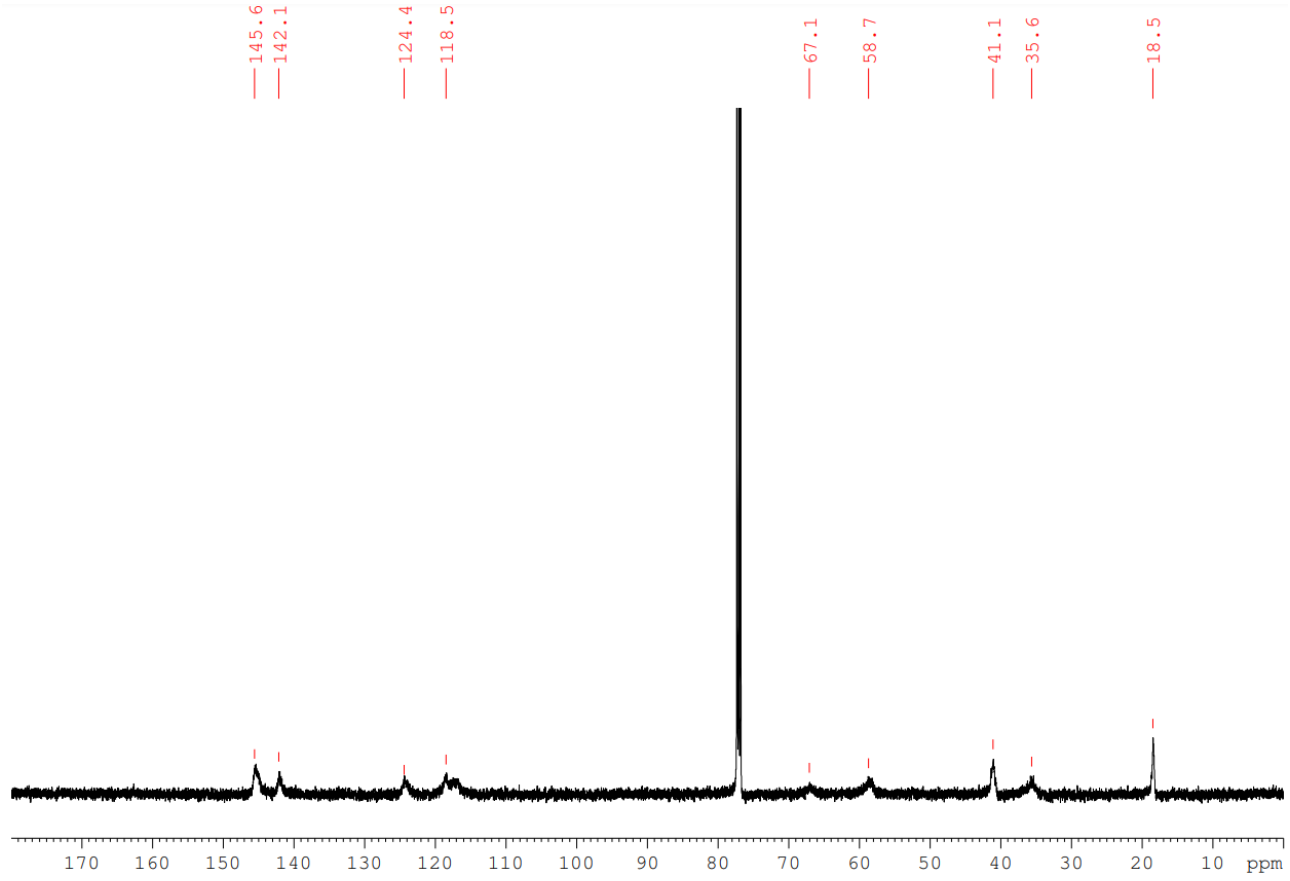

Figure S32 ^{13}C NMR spectra of **PIM-BTZ-1%** in $CDCl_3$.

TB-BTZ

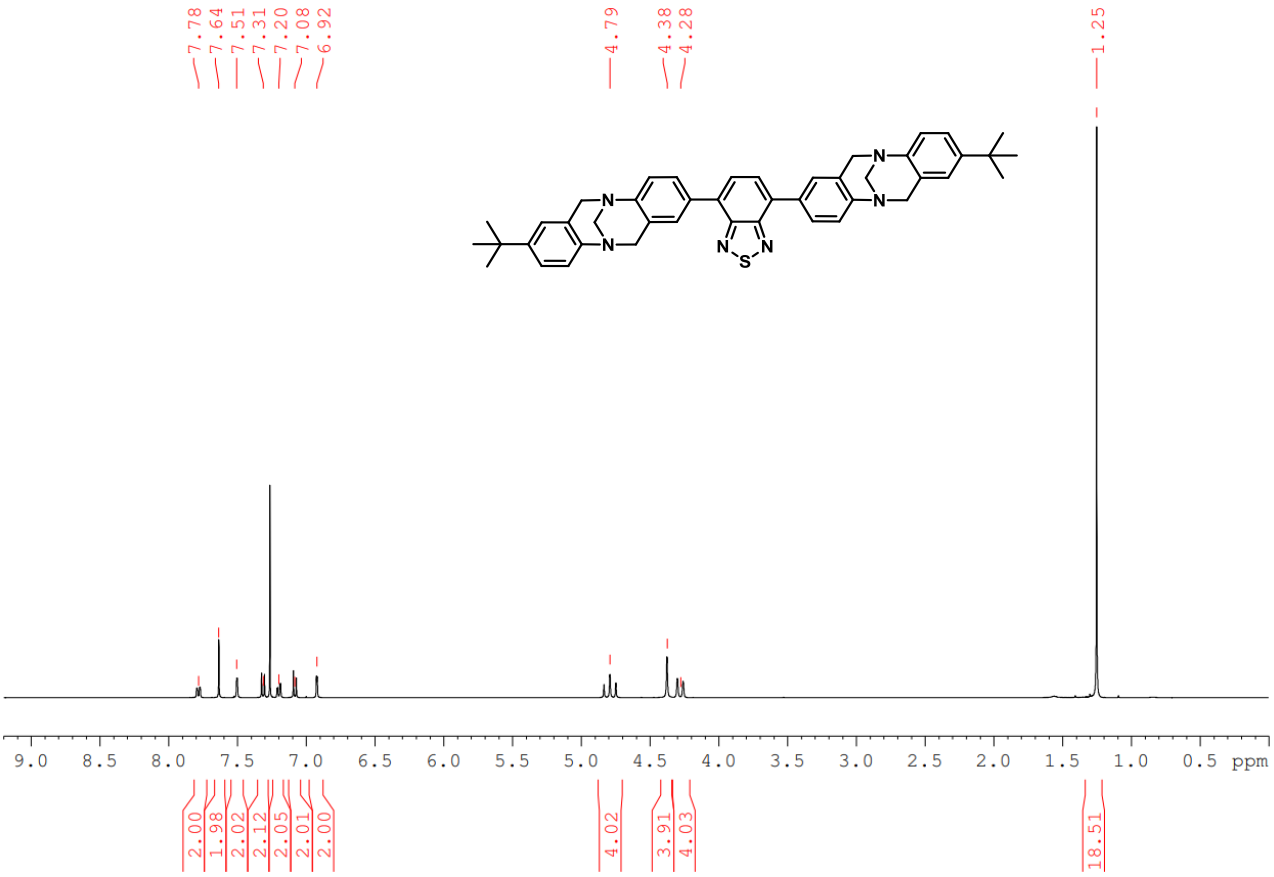

Figure S33 ^{1}H NMR spectra of **TB-BTZ** in $CDCl_3$.

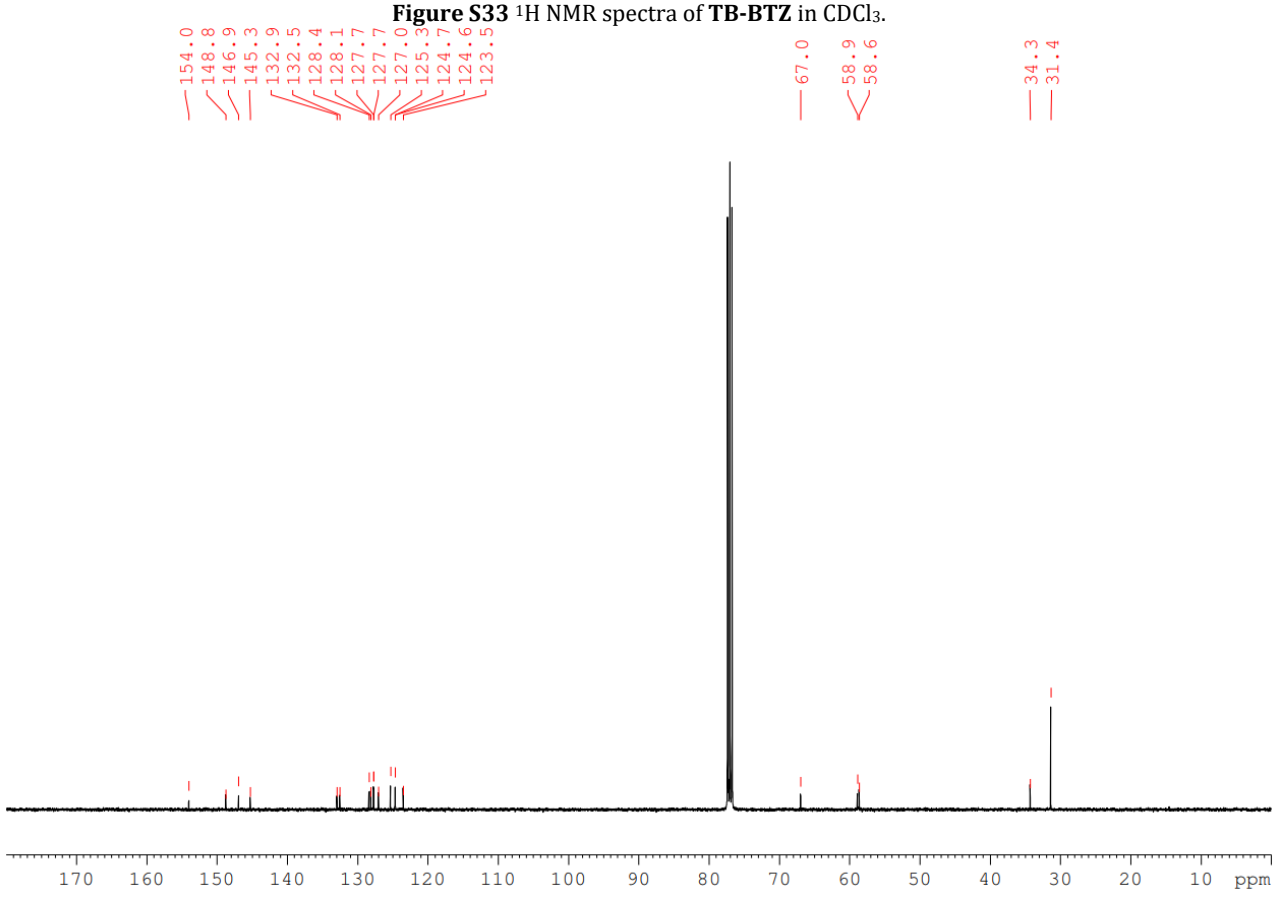

Figure S34 ^{13}C NMR spectra of **TB-BTZ** in $CDCl_3$.

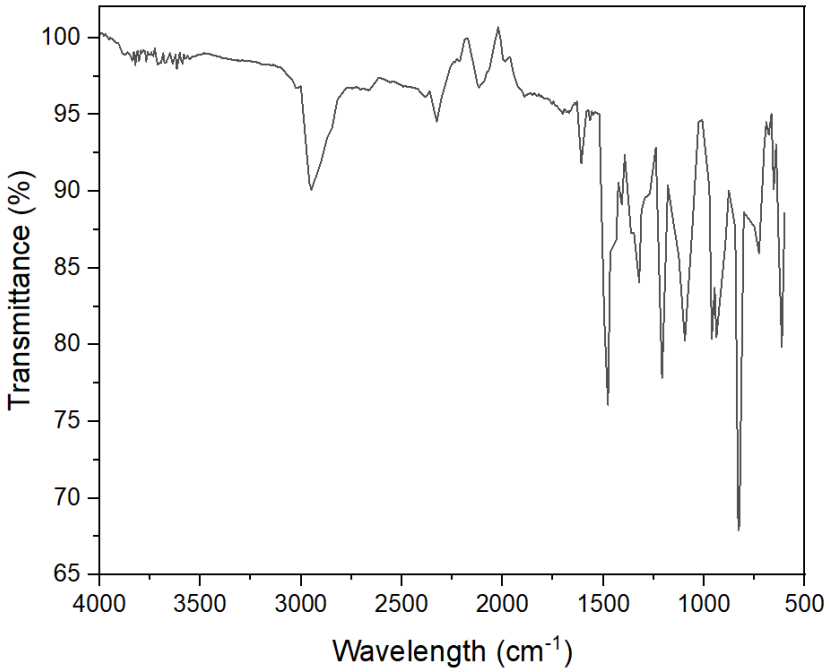

Figure S35 IR spectra of **TB-BTZ**.

Triphenylphosphine oxide

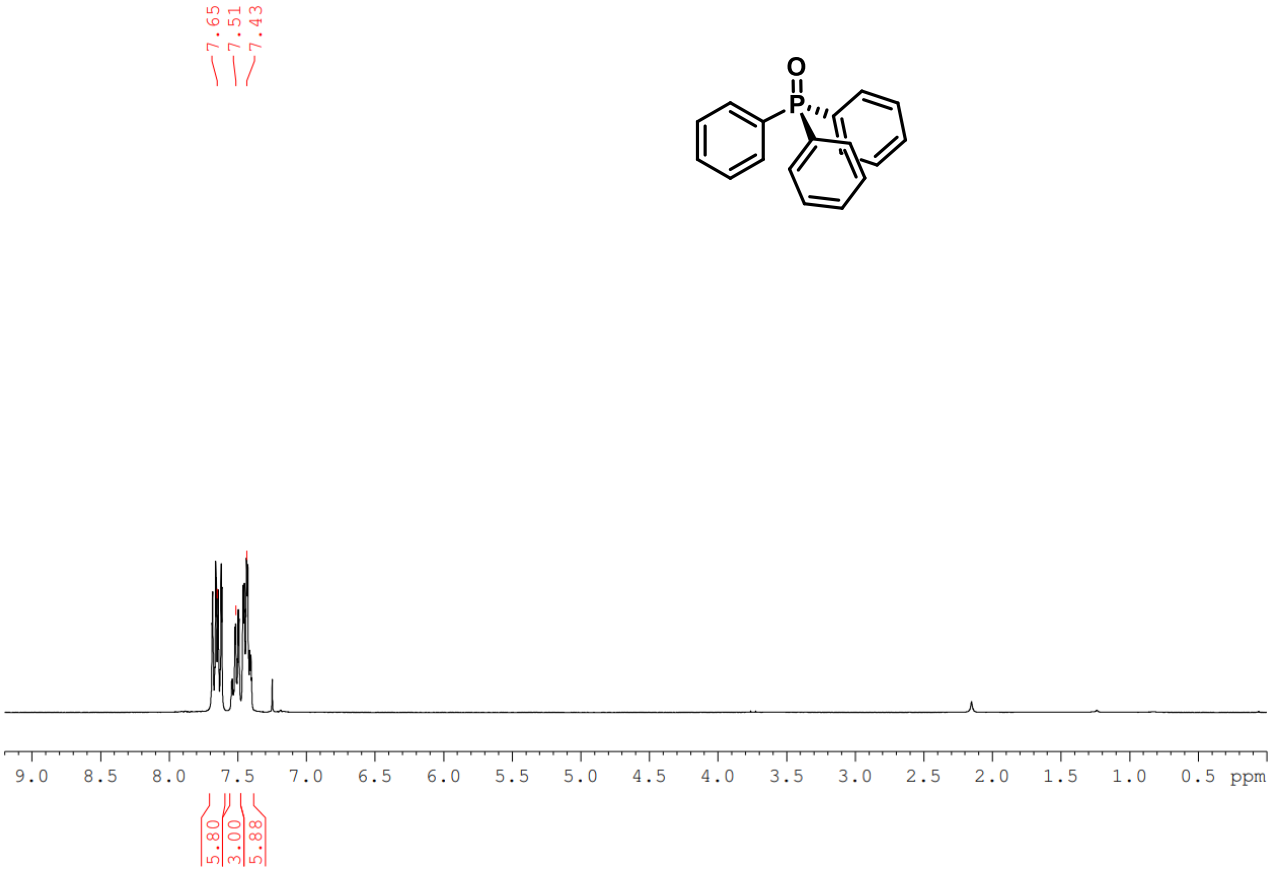

Figure S36 ^{1}H NMR spectra of triphenylphosphine oxide in $CDCl_3$.

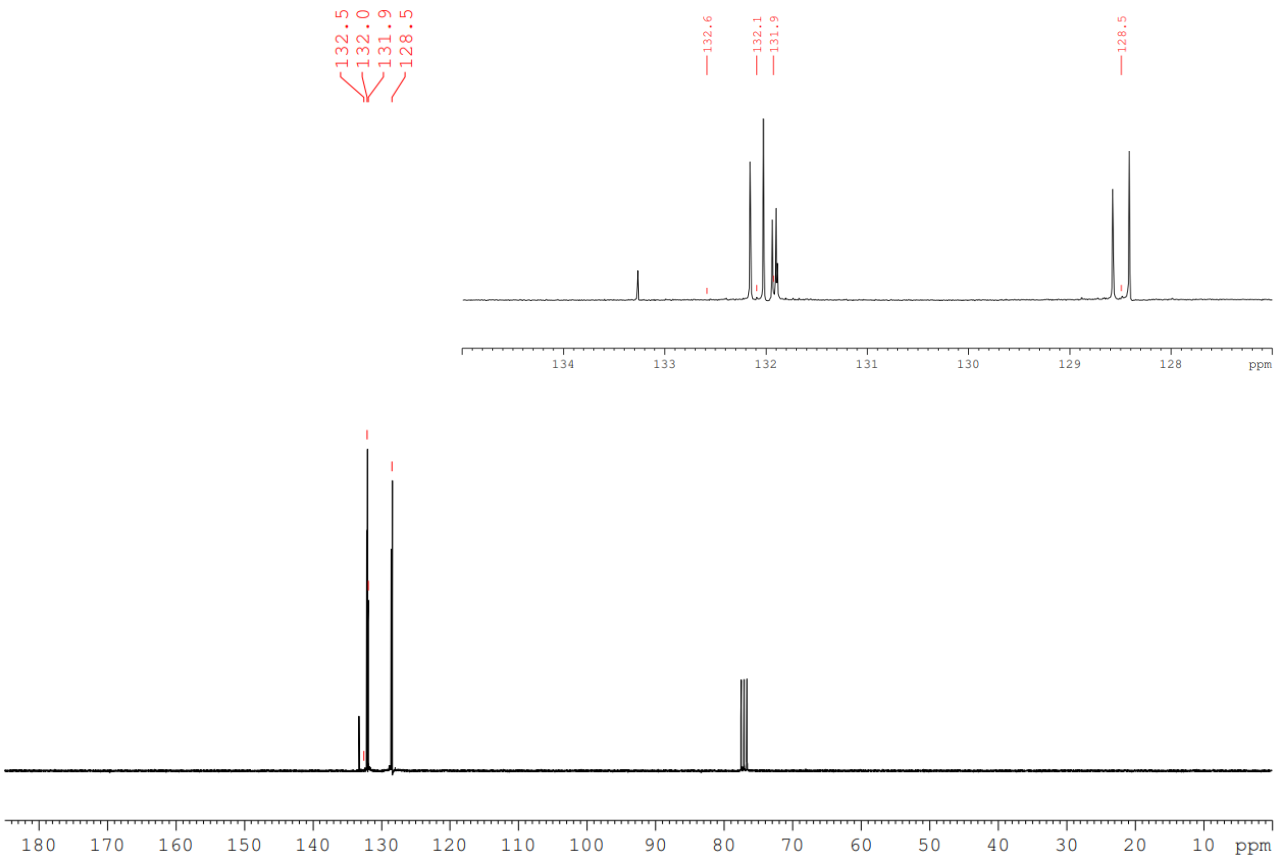

Figure S37 ^{13}C NMR spectra of triphenylphosphine oxide in $CDCl_3$.

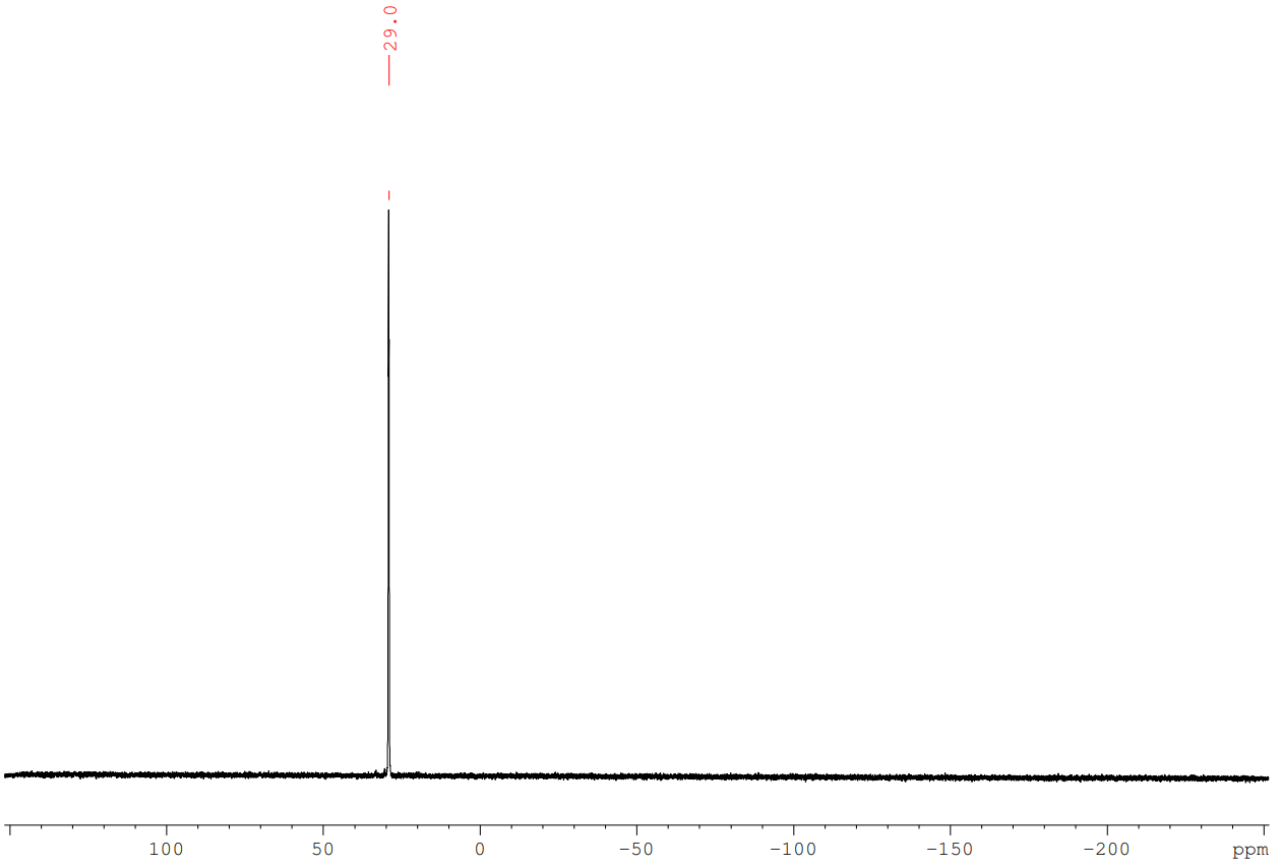

Figure S38 ^{31}P NMR spectra of triphenylphosphine oxide in $CDCl_3$.

Tri-*p*-tolylphosphine oxide

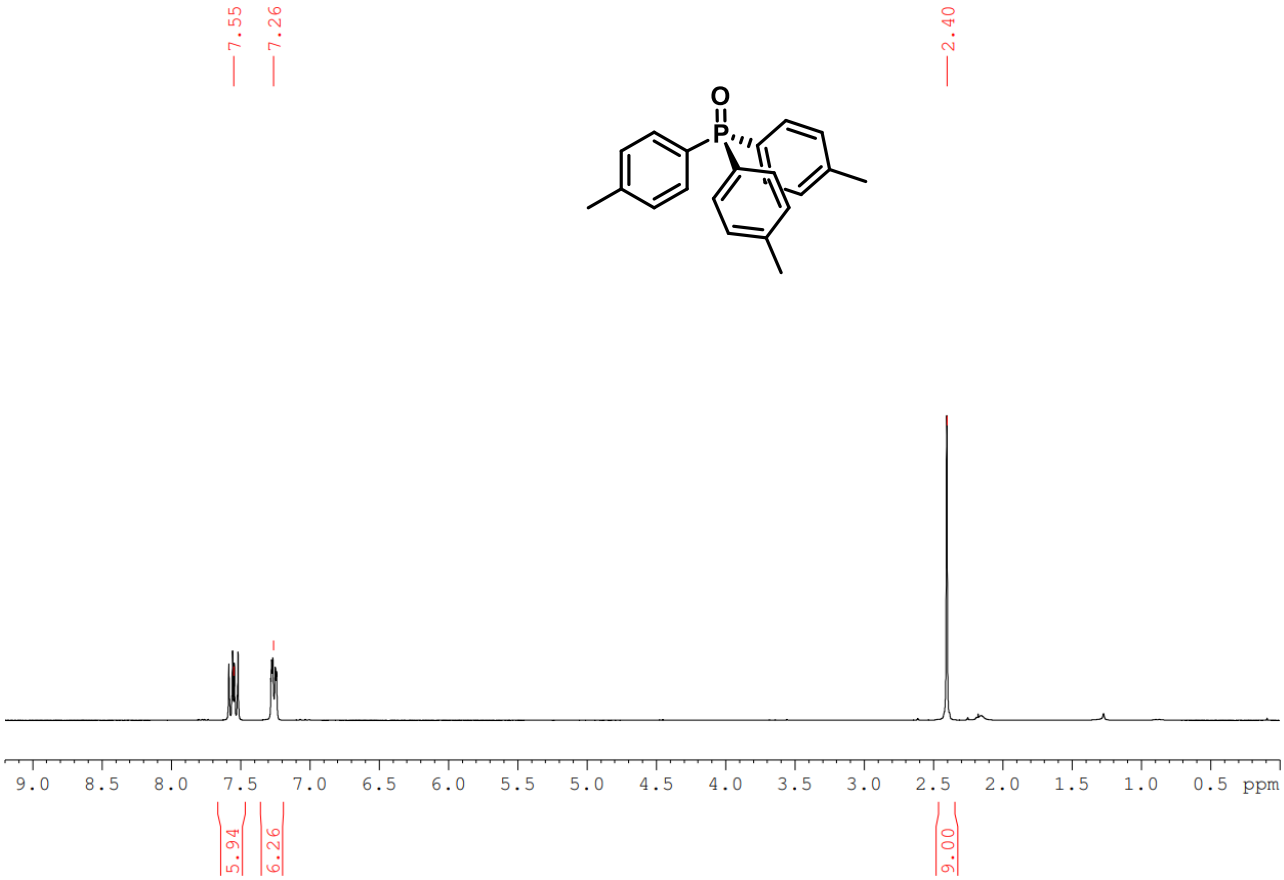

Figure S39 ^{1}H NMR spectra of tri-*p*-tolylphosphine oxide in $CDCl_3$.

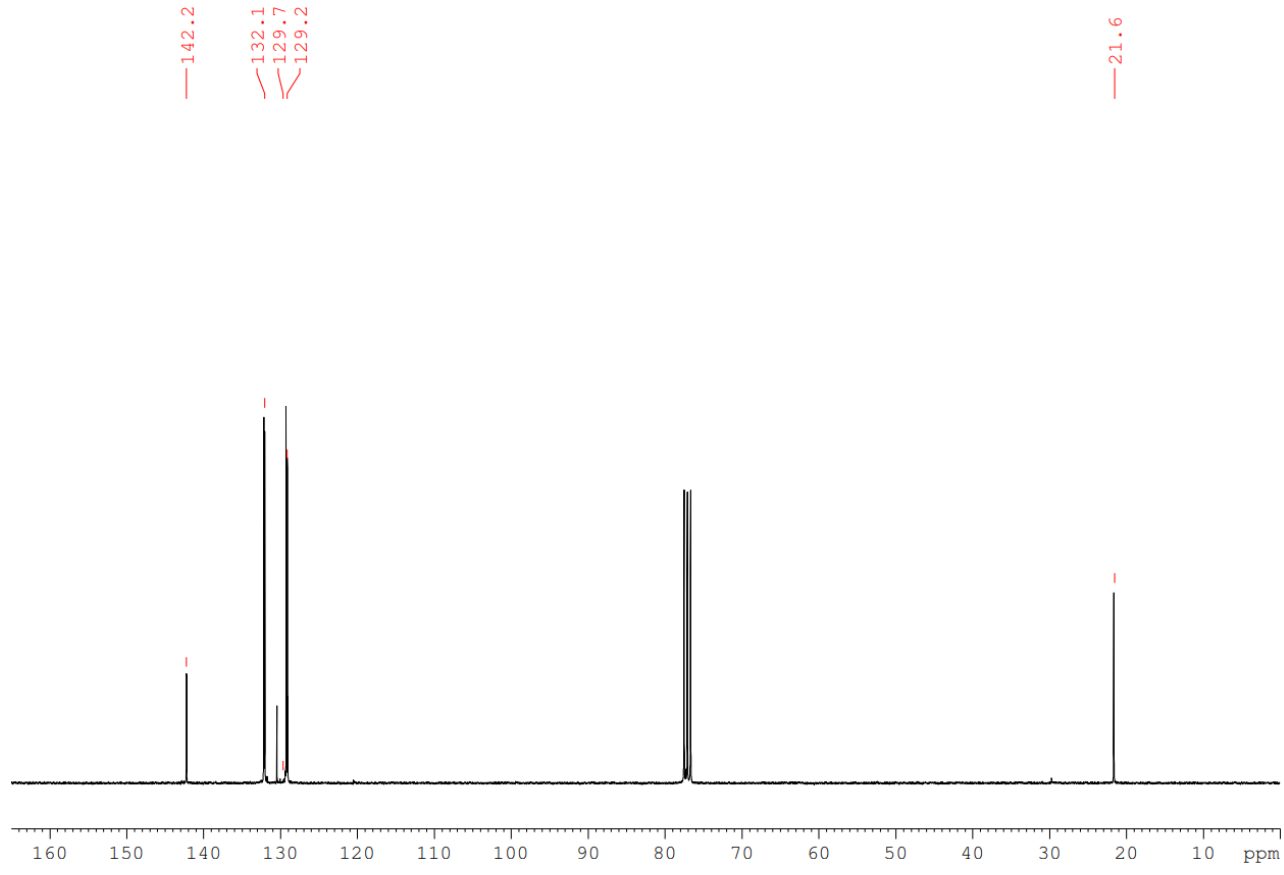

Figure S40 ^{13}C NMR spectra of tri-*p*-tolylphosphine oxide in $CDCl_3$.

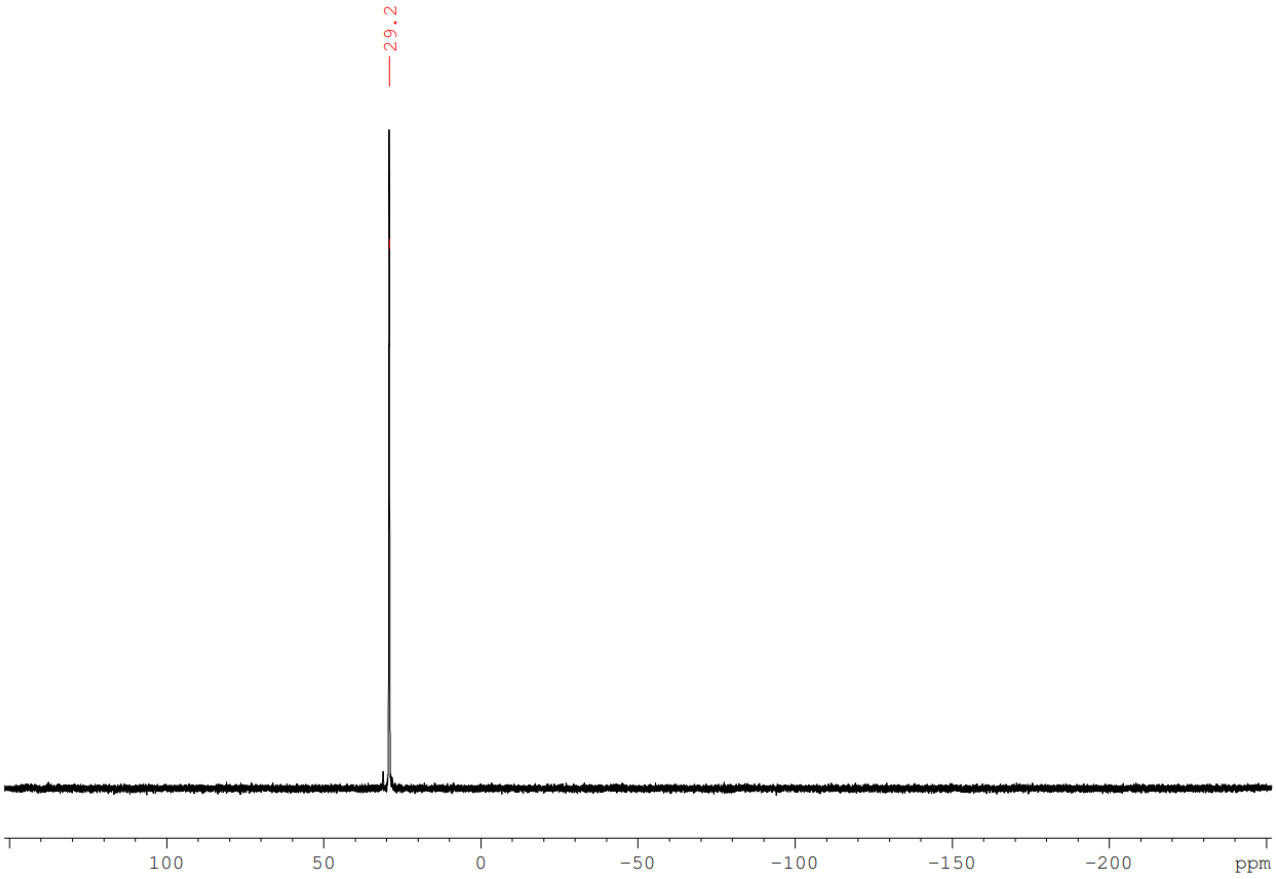

Figure S41 ^{31}P NMR spectra of tri-*p*-tolylphosphine oxide in $CDCl_3$.

Trimesitylphosphine oxide

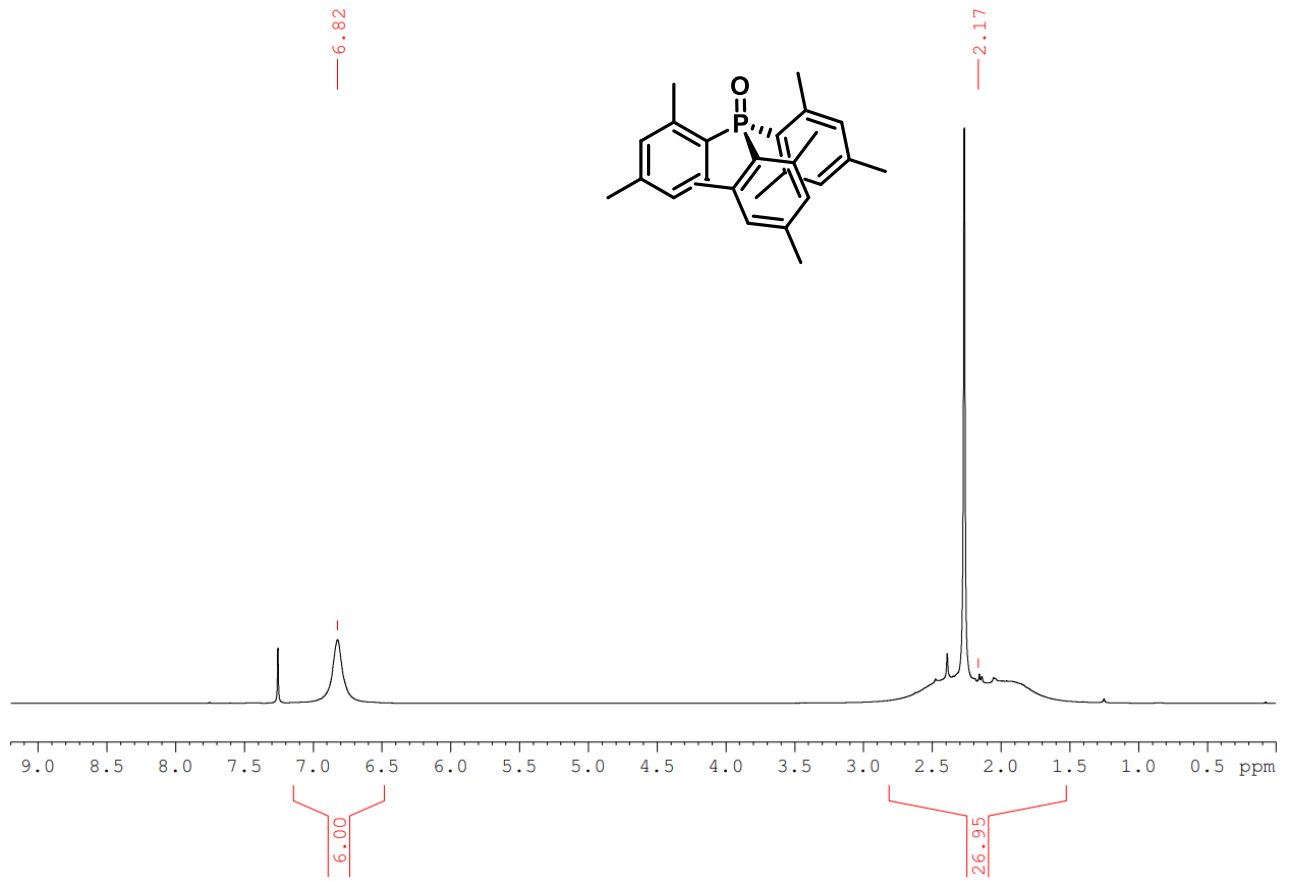

Figure S42 ^{1}H NMR spectra of trimesitylphosphine oxide in $CDCl_3$.

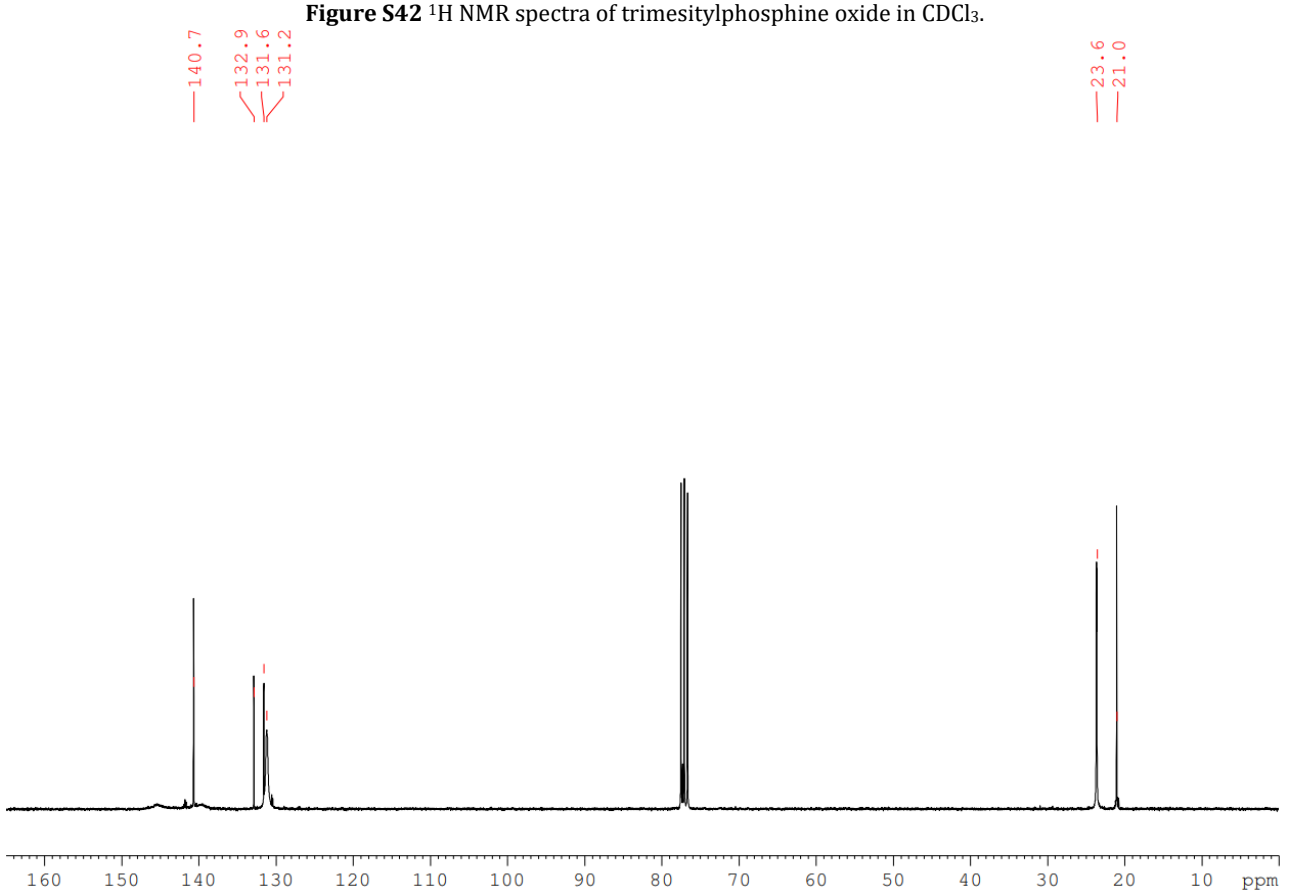

Figure S43 ^{13}C NMR spectra of trimesitylphosphine oxide in $CDCl_3$.

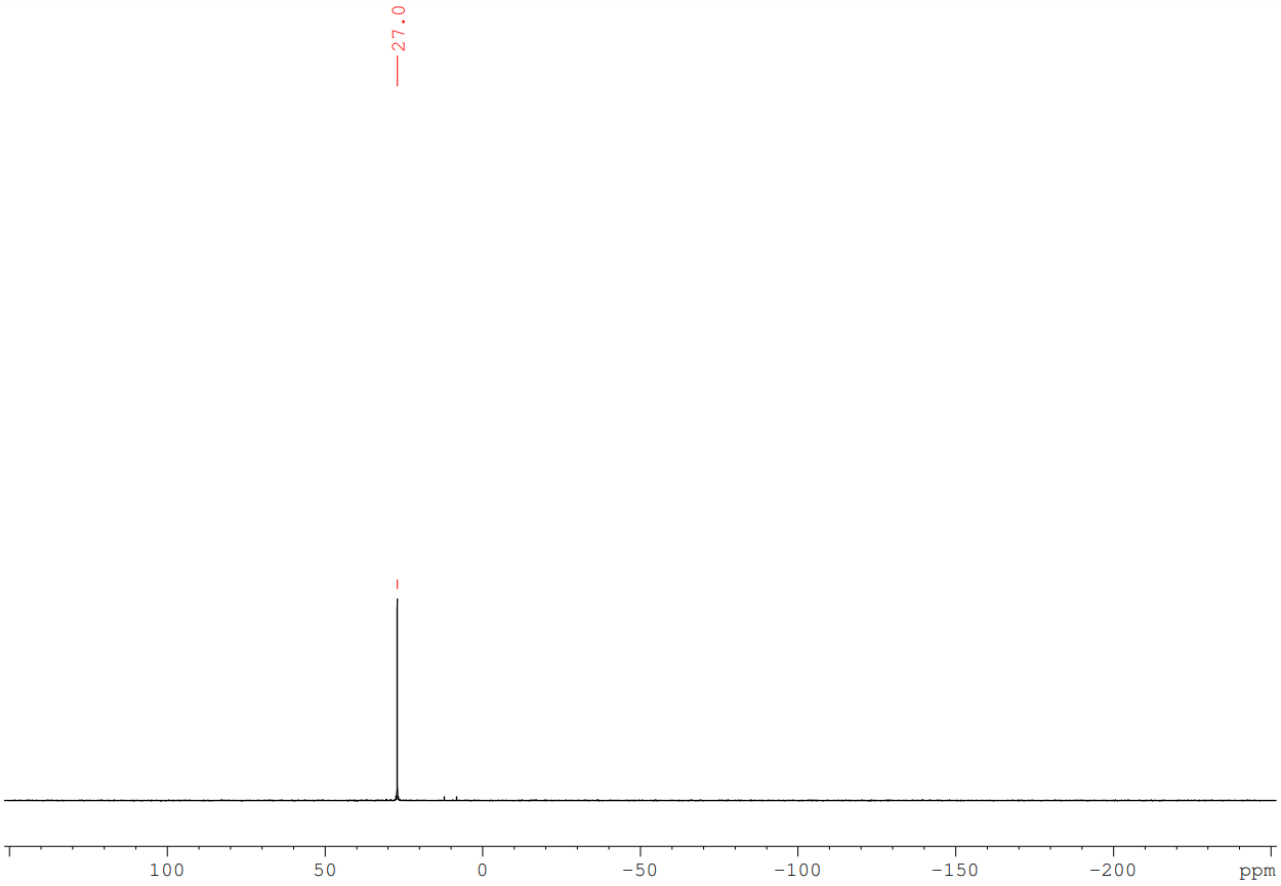

Figure S44 ^{31}P NMR spectra of trimesitylphosphine oxide in $CDCl_3$.

Tris(4-methoxyphenyl)phosphine oxide

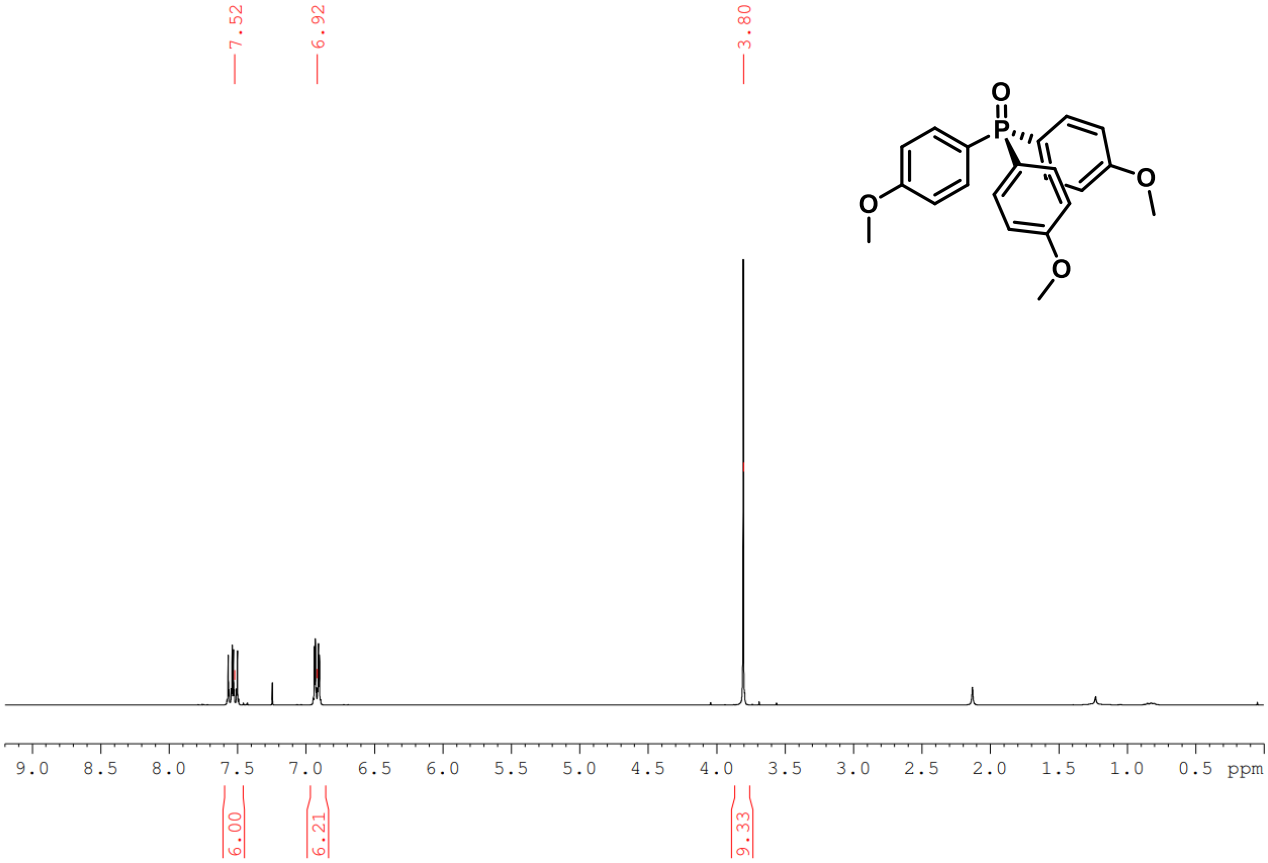

Figure S45 ^{1}H NMR spectra of tris(4-methoxyphenyl)phosphine oxide in $CDCl_3$.

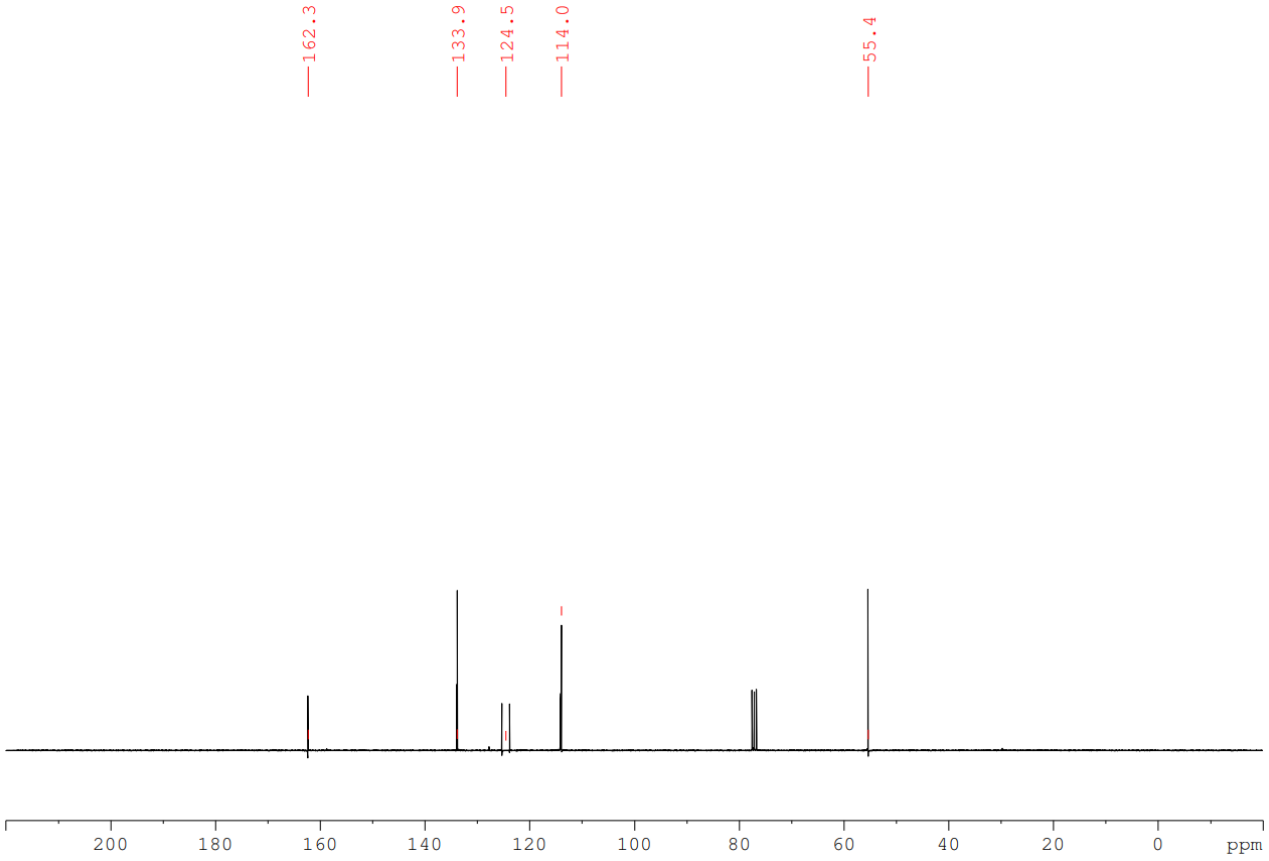

Figure S46 ^{1}H NMR spectra of tris(4-methoxyphenyl)phosphine oxide in $CDCl_3$.

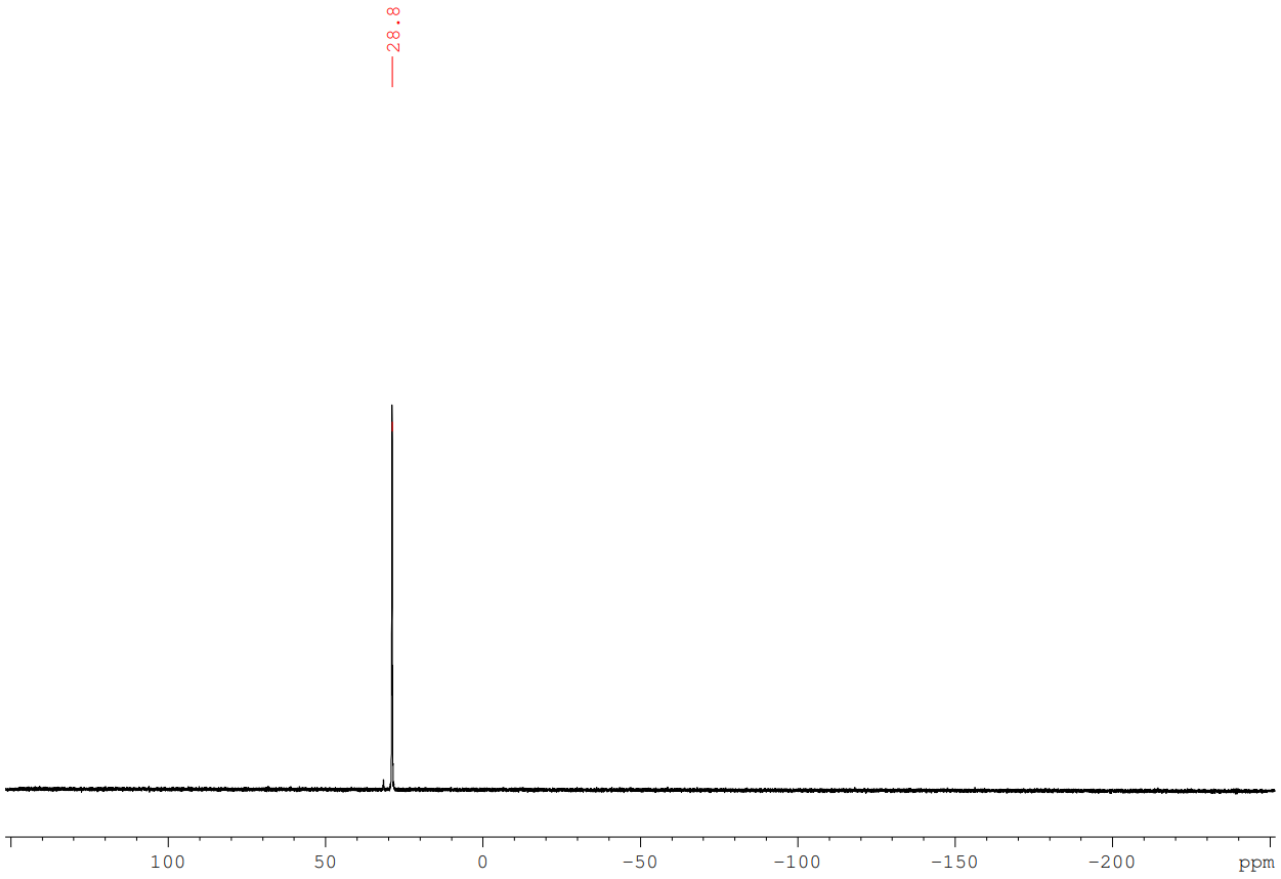

Figure S47 ^{31}P NMR spectra of tris(4-methoxyphenyl)phosphine oxide in $CDCl_3$.

Tris(4-fluorophenyl)phosphine oxide

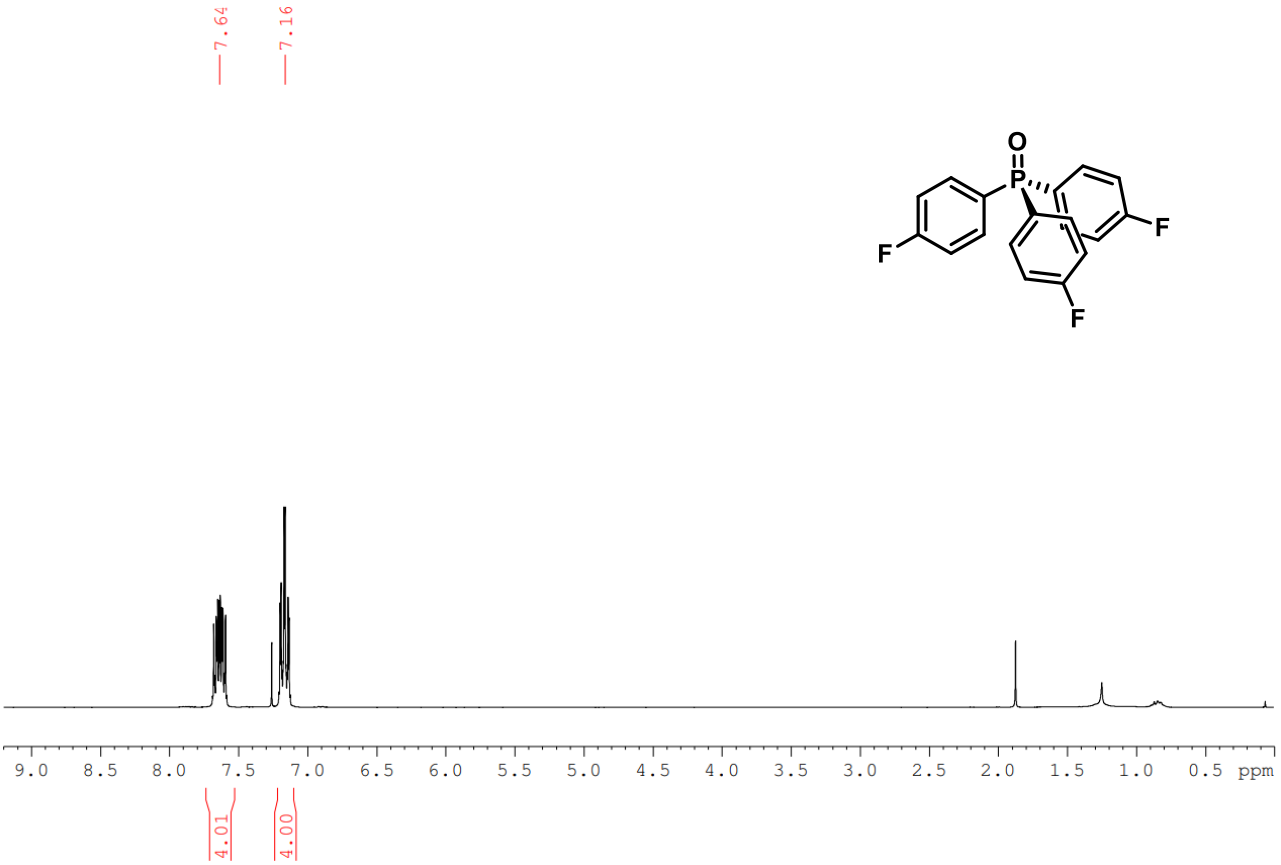

Figure S48 ^{1}H NMR spectra of tris(4-fluorophenyl)phosphine oxide in $CDCl_3$.

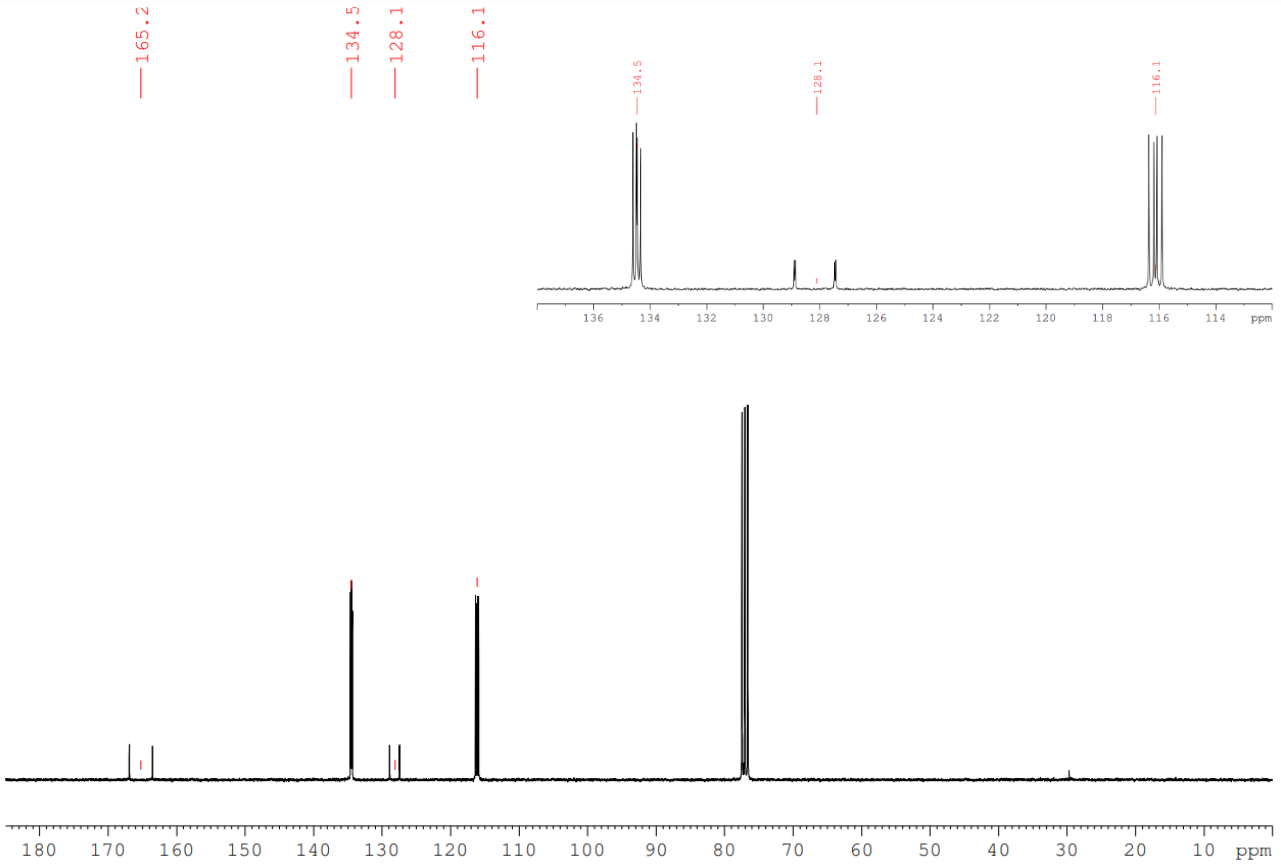

Figure S49 ^{13}C NMR spectra of tris(4-fluorophenyl)phosphine oxide in $CDCl_3$.

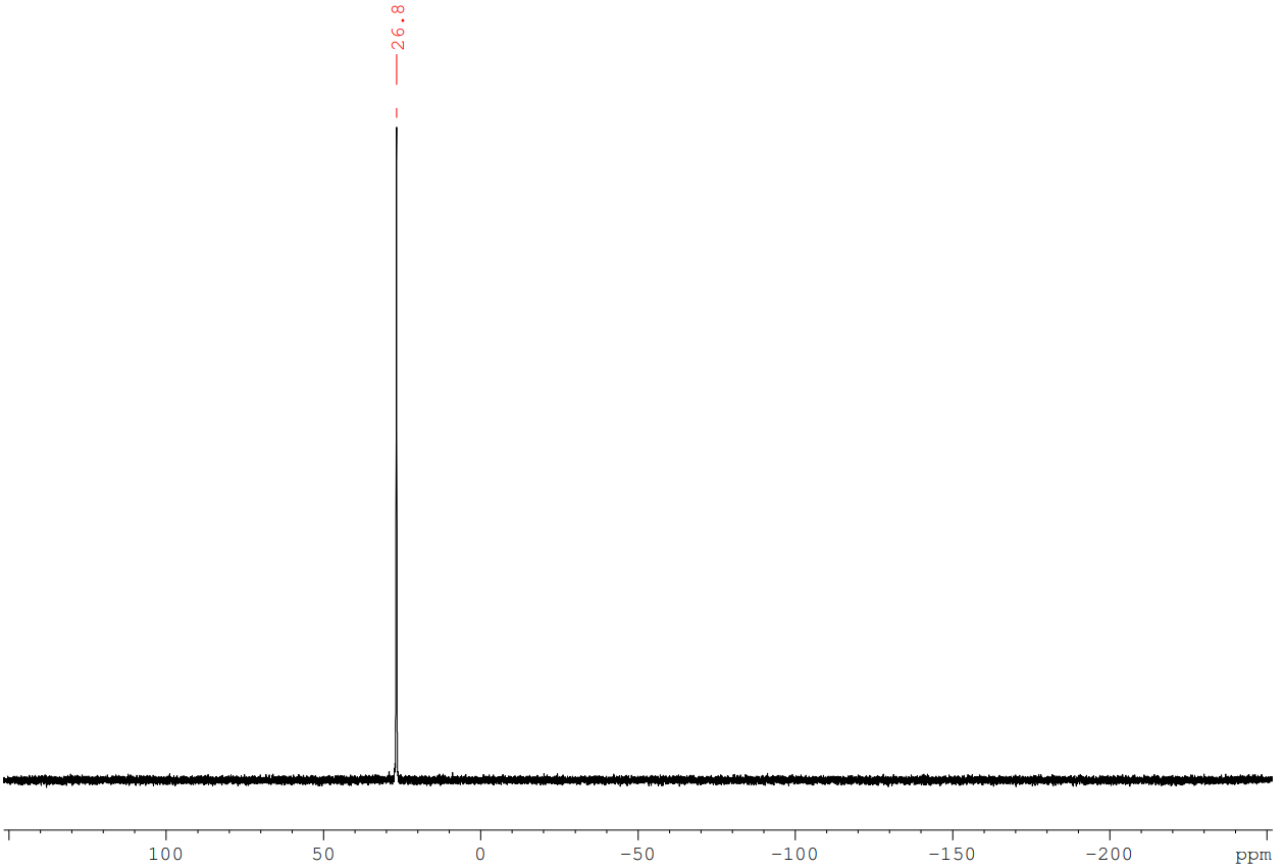

Figure S50 ^{31}P NMR spectra of tris(4-fluorophenyl)phosphine oxide in $CDCl_3$.

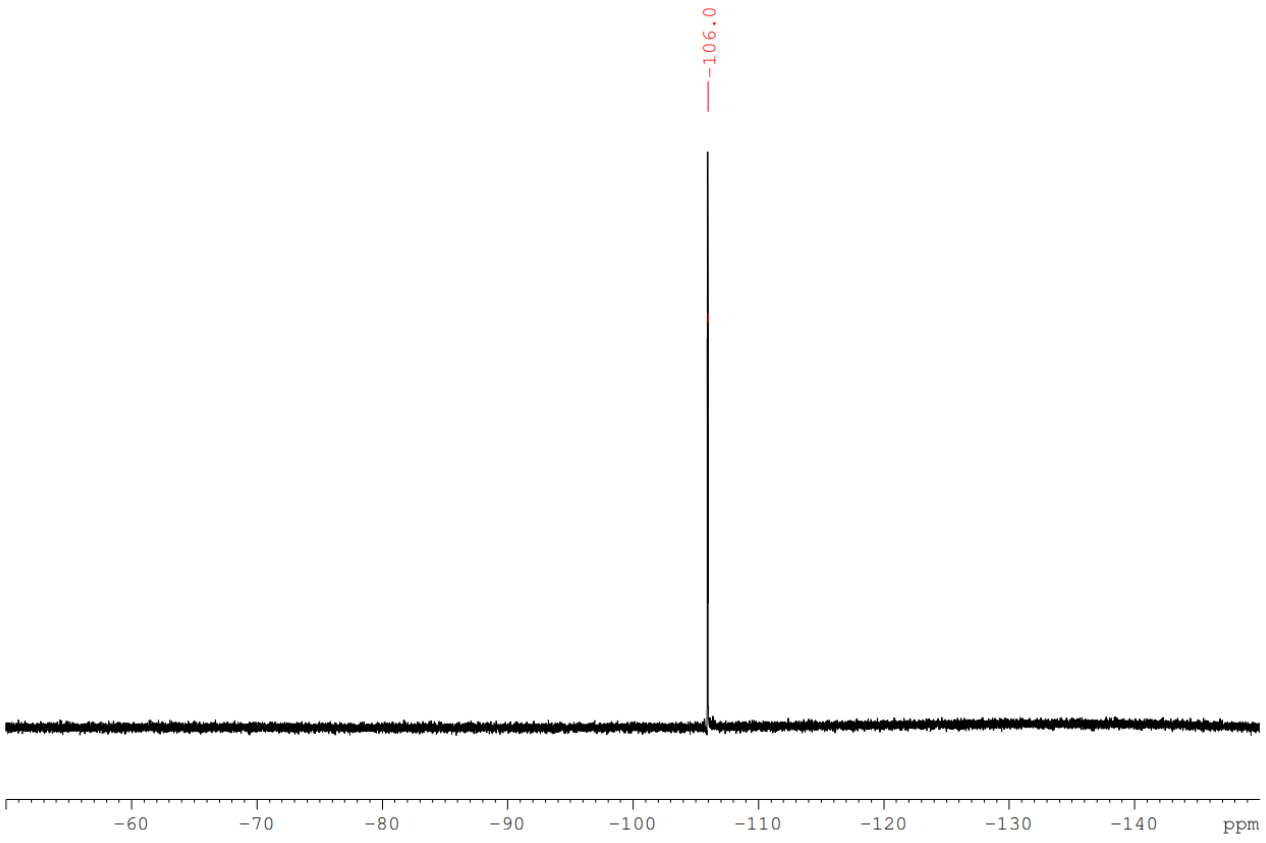

Figure S51 ^{19}F NMR spectra of tris(4-fluorophenyl)phosphine oxide in $CDCl_3$.

8. References

1 M. Ranger, D. Rondeau and M. Leclerc, *Macromolecules*, 1997, **30**, 7686–7691.

2 J. P. Heiskanen, P. Vivo, N. M. Saari, T. I. Hukka, T. Kastinen, K. Kaunisto, H. J. Lemmetyinen and O. E. O. Hormi, *J. Org. Chem.*, 2016, **81**, 1535–1546.

3 D. Taylor, T. Malcomson, A. Zhakeyev, S.-X. Cheng, G. M. Rosair, J. Marques-Hueso, Z. Xu, M. J. Paterson, S. J. Dalgarno and F. Vilela, *Org. Chem. Front.*, 2022, **9**, 5473–5484.

4 M. Carta, R. Malpass-Evans, M. Croad, Y. Rogan, J. C. Jansen, P. Bernardo, F. Bazzarelli and N. B. McKeown, *Science*, 2013, **339**, 303–307.

5 P. M. Budd, B. S. Ghanem, S. Makhseed, N. B. McKeown, K. J. Msayib and C. E. Tattershall, *Chem. Commun.*, 2004, **4**, 230–231.

6 C. Cheng, X. Wang, Y. Lin, L. He, J. X. Jiang, Y. Xu and F. Wang, *Polym. Chem.*, 2018, **9**, 4468–4475.

7 J. Byun, K. Landfester and K. A. I. Zhang, *Chem. Mater.*, 2019, **31**, 3381–3387.

8 S. Ren, R. Dawson, D. J. Adams and A. I. Cooper, *Polym. Chem.*, 2013, **4**, 5585–5590.

9 R. Li, Z. J. Wang, L. Wang, B. C. Ma, S. Ghasimi, H. Lu, K. Landfester and K. A. I. Zhang, *ACS Catal.*, 2016, **6**, 1113–1121.

10 S. Wang, Q. Sun, W. Chen, Y. Tang, B. Aguila, Y. Pan, A. Zheng, Z. Yang, L. Wojtas, S. Ma and F. S. Xiao, *Matter*, 2020, **2**, 416–427.

11 S. Yang, X. Li, Y. Qin, Y. Cheng, W. Fan, X. Lang, L. Zheng and Q. Cao, *ACS Appl. Mater. Interfaces*, 2021, **13**, 29471–29481.

12 S. Goswami, C. E. Miller, J. L. Logsdon, C. T. Buru, Y.-L. Wu, D. N. Bowman, T. Islamoglu, A. M. Asiri, C. J. Cramer, M. R. Wasielewski, J. T. Hupp and O. K. Farha, *ACS Appl. Mater. Interfaces*, 2017, **9**, 19535–19540.

13 J.-K. Jin, K. Wu, X.-Y. Liu, G.-Q. Huang, Y.-L. Huang, D. Luo, M. Xie, Y. Zhao, W. Lu, X.-P. Zhou, J. He and D. Li, *J. Am. Chem. Soc.*, 2021, **143**, 21340–21349.

14 A. Vázquez-Romero, N. Kielland, M. J. Arévalo, S. Preciado, R. J. Mellanby, Y. Feng, R. Lavilla and M. Vendrell, *J. Am. Chem. Soc.*, 2013, **135**, 16018–16021.

15 M. Kondo and T. Agou, *Chem. Commun.*, 2022, **58**, 5001–5004.

16 C. Laye, J. Lusseau, F. Robert and Y. Landais, *Adv. Synth. Catal.*, 2021, **363**, 3035–3043.

17 H. Urakami, K. Zhang and F. Vilela, *Chem. Commun.*, 2013, **49**, 2353–2355.

18 E. Runge and E. K. U. Gross, *Phys. Rev. Lett.*, 1984, **52**, 997–1000.

19 P. Hohenberg and W. Kohn, *Phys. Rev.*, 1964, **136**, B864–B871.

20 W. Kohn and L. J. Sham, *Phys. Rev.*, 1965, **140**, A1133–A1138.

21 M. J. Frisch, G. W. Trucks, H. B. Schlegel, G. E. Scuseria, M. A. Robb, J. R. Cheeseman, G.

Scalmani, V. Barone, G. A. Petersson, H. Nakatsuji, X. Li, M. Caricato, A. V. Marenich, J. Bloino, B. G. Janesko, R. Gomperts, B. Mennucci, H. P. Hratchian, J. V. Ortiz, A. F. Izmaylov, J. L. Sonnenberg, D. Williams-Young, F. Ding, F. Lipparini, F. Egidi, J. Goings, B. Peng, A. Petrone, T. Henderson, D. Ranasinghe, V. G. Zakrzewski, J. Gao, N. Rega, G. Zheng, W. Liang, M. Hada, M. Ehara, K. Toyota, R. Fukuda, J. Hasegawa, M. Ishida, T. Nakajima, Y. Honda, O. Kitao, H. Nakai, T. Vreven, K. Throssell, J. A. Montgomery, Jr., J. E. Peralta, F. Ogliaro, M. J. Bearpark, J. J. Heyd, E. N. Brothers, K. N. Kudin, V. N. Staroverov, T. A. Keith, R. Kobayashi, J. Normand, K. Raghavachari, A. P. Rendell, J. C. Burant, S. S. Iyengar, J. Tomasi, M. Cossi, J. M. Millam, M. Klene, C. Adamo, R. Cammi, J. W. Ochterski, R. L. Martin, K. Morokuma, O. Farkas, J. B. Foresman, and D. J. Fox, Gaussian 16, Revision C.02, Inc., Wallingford CT.

22 C. Lee, W. Yang and R. G. Parr, *Phys. Rev. B*, 1988, **37**, 785–789.

23 A. D. Becke, *J. Chem. Phys.*, 1993, **98**, 1372–1377.

24 P. J. Stephens, F. J. Devlin, C. F. Chabalowski and M. J. Frisch, *J. Phys. Chem.*, 1994, **98**, 11623–11627.

25 T. Yanai, D. P. Tew and N. C. Handy, *Chem. Phys. Lett.*, 2004, **393**, 51–57.

26 A. V. Marenich, C. J. Cramer and D. G. Truhlar, *J. Phys. Chem. B*, 2009, **113**, 6378–6396.

27 T. H. Dunning, *J. Chem. Phys.*, 1989, **90**, 1007–1023.

28 D. E. Woon and T. H. Dunning, *J. Chem. Phys.*, 1993, **98**, 1358–1371.

29 D. Taylor, T. Malcomson, A. Zhakeyev, G. M. Rosair, M. J. Paterson, J. Marques-Hueso, S. J. Dalgarno and F. Vilela, *RSC Adv.*, 2023, **13**, 5826–5832.

30 S. Hirata and M. Head-Gordon, *Chem. Phys. Lett.*, 1999, **314**, 291–299.